




Effect of number of diffusion-encoding directions in diffusion metrics of 5-year-olds using tract-based spatial statistical analysis

Venla Kumpulainen¹  | Harri Merisaari^{1,2}  | Anni Copeland¹ | Eero Silver¹ | Elmo P. Pulli¹  | John D. Lewis³ | Ekaterina Saukko² | Jani Saunavaara⁴ | Linnea Karlsson^{1,5,6,7} | Hasse Karlsson^{1,6,7} | Jetro J. Tuuluri^{1,6,8}

¹FinnBrain Birth Cohort Study, Turku Brain and Mind Center, Department of Clinical Medicine, University of Turku, Turku, Finland

²Department of Radiology, Turku University Hospital, Turku, Finland

³Montreal Neurological Institute, McGill University, Montreal, Quebec, Canada

⁴Department of Medical Physics, Turku University Hospital and University of Turku, Turku, Finland

⁵Department of Paediatrics and Adolescent Medicine, Turku University Hospital and University of Turku, Turku, Finland

⁶Department of Psychiatry, Turku University Hospital and University of Turku, Turku, Finland

⁷Centre for Population Health Research, Turku University Hospital and University of Turku, Turku, Finland

⁸Turku Collegium for Science and Medicine, University of Turku, Turku, Finland

Correspondence

Venla Kumpulainen, FinnBrain Birth Cohort Study, Turku Brain and Mind Center, Department of Clinical Medicine, University of Turku, Kiinamylynkatu 8-10, FinnBrain Study, Medisiina A Building, 20520 Turku, Finland.
Email: veviku@utu.fi

Funding information

Academy of Finland; Cultural Foundation of Finland, Grant/Award Number: 00190572; Jane ja Aatos Erkkö Foundation; Juho Vainio Foundation;

Abstract

Methodological aspects and effects of different imaging parameters on DTI (diffusion tensor imaging) results and their reproducibility have been recently studied comprehensively in adult populations. Although MR imaging of children's brains has become common, less interest has been focussed on researching whether adult-based optimised parameters and pre-processing protocols can be reliably applied to paediatric populations. Furthermore, DTI scalar values of preschool aged children are rarely reported. We gathered a DTI dataset from 5-year-old children ($N = 49$) to study the effect of the number of diffusion-encoding directions on the reliability of resultant scalar values

Abbreviations: ACR, anterior corona radiata; AD, axial diffusivity; ALIC, anterior limb of internal capsule; BCC, body of corpus callosum; BET, Brain Extraction Tool; CG, cingulate gyrus; CING, cingulum; CP, cerebral peduncle; CST, corticospinal tract; DTI, diffusion tensor imaging; EC, external capsule; FA, fractional anisotropy; FDR, false discovery rate; FOV, field of view; FSL, FMRIB Software Library; GCC, genu of corpus callosum; ICC, intraclass correlation coefficient; ILF/IFOF, inferior longitudinal fasciculus/inferior fronto-occipital fasciculus; MD, mean diffusivity; MNI, Montreal Neurological Institute; MRI, magnetic resonance imaging; NA, not available; PCR, posterior corona radiata; PLIC, posterior limb of internal capsule; PTR/OT, posterior thalamic radiation/optic tract; RD, radial diffusivity; r1 IC, retrolenticular internal capsule; ROI, region of interest; SCC, splenium of corpus callosum; SCR, superior corona radiata; SD, standard deviation; SE-EPI, spin echo-echo planar imaging; SFOF, superior fronto-occipital fasciculus; SLF, superior longitudinal fasciculus; SNR, signal-to-noise ratio; TBSS, tract-based spatial statistics; TE, time of echo; TR, time of repetition; UNC, uncinate fasciculus; VBA, voxel-based analysis; WM, white matter.

Anni Copeland, Eero Silver, and Elmo P. Pulli contributed equally to this study.

This is an open access article under the terms of the [Creative Commons Attribution-NonCommercial-NoDerivs](https://creativecommons.org/licenses/by-nc-nd/4.0/) License, which permits use and distribution in any medium, provided the original work is properly cited, the use is non-commercial and no modifications or adaptations are made.

© 2022 The Authors. *European Journal of Neuroscience* published by Federation of European Neuroscience Societies and John Wiley & Sons Ltd.

Signe ja Ane Gyllenberg Foundation;
Suomen Aivosäätiö; The Finnish Medical
Foundation; Turunmaan Duodecim -seura

Edited by: Sophie Molholm

with TBSS (tract-based spatial statistics) method. Additionally, the potential effect of within-scan head motion on DTI scalars was evaluated. Reducing the number of diffusion-encoding directions deteriorated both the accuracy and the precision of all DTI scalar values. To obtain reliable scalar values, a minimum of 18 directions for TBSS was required. For TBSS fractional anisotropy values, the intraclass correlation coefficient with two-way random-effects model (ICC[2,1]) for the subsets of 6 to 66 directions ranged between 0.136 [95%CI 0.0767;0.227] and 0.639 [0.542;0.740], whereas the corresponding values for subsets of 18 to 66 directions were 0.868 [0.815;0.913] and 0.995 [0.993;0.997]. Following the exclusion of motion-corrupted volumes, minor residual motion did not associate with the scalar values. A minimum of 18 diffusion directions is recommended to result in reliable DTI scalar results with TBSS. We suggest gathering extra directions in paediatric DTI to enable exclusion of volumes with motion artefacts and simultaneously preserve the overall data quality.

KEYWORDS

diffusion encoding directions, DTI, paediatric MR imaging, TBSS

1 | INTRODUCTION

Diffusion tensor imaging (DTI) has been established as an informative tool in studying human brain white matter (WM) microstructure and connectivity during last decades (Pierpaoli et al., 1996). Although it provides feasible means to investigate brain features, including paediatric brain development, certain methodological limitations should be acknowledged. DTI scalar values (fractional anisotropy [FA], mean diffusivity [MD], radial diffusivity [RD] and axial diffusivity [AD]; Basser & Pierpaoli, 2011) reflect the underlying neural microstructure but lack specificity to fully differentiate between biological components of diffusion properties affected, for example, by myelination, axonal diameter, packing, kissing and crossing of fibres. Furthermore, making conclusions from the results of separate studies has become challenging and raised extensive discussion of DTI data reliability. A plethora of available parameter choices for researchers related to data acquisition, processing, analysis methods and their combinations coupled with incomplete methodological reporting inevitably reduces the comparability and reproducibility of DTI studies (Jones & Basser, 2004; Le Bihan et al., 2006).

DTI has relatively low signal-to-noise ratio (SNR) and is susceptible to artefacts in areas of magnetic field inhomogeneity (such as interfaces among brain, bone and air) because of within-scan movement and hardware properties (Basser & Jones, 2002). Additionally, the acquisition

protocol, including number of gradients (Jones, 2004; Landman et al., 2007), b values (Gao et al., 2009) and voxel resolution (Fujiwara et al., 2008), influences the resultant DTI scalar values. Several recent studies of adult populations have aimed to optimise and standardise the DTI protocol parameters especially regarding reliability of DTI scalar values. Improving image quality by averaging or increasing the number of diffusion-encoding gradient directions for more robust tensor estimation is utilisable approaches, yet they both also denote longer acquisition times. In previous adult-population studies, rejecting diffusion-encoding gradient directions has been indicated to deteriorate the accuracy (systematic bias) and precision (deviation around the bias) of DTI scalar values (Barrio-Arranz et al., 2015; Chen et al., 2015; Giannelli et al., 2010; Sairanen et al., 2017). As a general trend, decreasing the number of directions commonly overestimates the FA values (Barrio-Arranz et al., 2015; Chen et al., 2015; Heiervang et al., 2006), and this phenomenon is emphasised in areas with low FA (Sairanen et al., 2017), typically in peripheral WM regions with most anatomical variance and partial volume effects. The dependence of FA values on the number diffusion-encoding directions is saturated towards higher numbers, and after 30 directions, it has been shown to have little effect on DTI scalars (Jones, 2004). In addition to the number, also the non-uniform sampling of gradient directions may alter DTI estimates (Landman et al., 2007). Similar studies replicating the effect of the number of diffusion-encoding

directions on DTI scalars have not been carried out in children.

Recent paediatric DTI studies have provided essential insight into WM tract development (Lebel et al., 2017). However, despite parallel results, the numeric range of individual DTI scalar values between separate studies is broad (Table 1). One apparent explanatory factor for differences between separate studies is the use of different MR scanners and imaging protocols. Although systematic bias present in a dataset does not influence the conclusions made from group-comparisons or correlation analyses, variability among separate datasets interferes with producing reliable estimations of biological reference values to guide advances in research and hinder future clinical applications. Even though there has been a clear trend towards increasing the number of collected diffusion directions in paediatric DTI, the final quantity of directions (or their spatial distribution) after quality control is rarely reported (Farah et al., 2020; Hutton et al., 2020a, 2020b; Lebel et al., 2016; Rollins et al., 2010; Taki et al., 2013; Wier et al., 2019). Furthermore, there are certain specific issues related to paediatric DTI requiring additional attention, such as involuntary motion during scanning (Stephens et al., 2020). To the best of our knowledge, guidelines for the minimum number of directions for reliable results have not yet been defined in paediatric population studies. Prior studies have frequently included wide age ranges in addition to publishing only derived statistics without exact diffusion values, leading to a gap of knowledge in normative characteristics of preschool-aged children's WM tracts. Consequently, there is a dire need to address this issue within the context of the developing brain.

In the current study, we manipulated the number of diffusion-encoding directions (whilst maximising the angular resolution) and characterised these effects on resultant diffusion scalar values (FA, MD, AD and RD) among 5-year-old typically developing children. Our main objective was therefore to provide an optimised pre-processing protocol and thus make between-study comparisons more straightforward in the future. We also provided a full description of WM tract scalar values in our sample and reported the effect of within-scan head motion on the scalar values.

2 | MATERIALS AND METHODS

This study was reviewed and approved by the Ethics Committee of the Hospital District of Southwest Finland ([07.08.2018] §330, ETMK: 31/180/2011), and performed in accordance with the Declaration of Helsinki.

2.1 | Participants

The families were recruited as part of the FinnBrain Birth Cohort Study (www.finnbrain.fi). The study population consisted of a subset of 110 families who agreed to participate in the magnetic resonance imaging (MRI) visit arranged at the age of 5 years between October 2017 and March 2021 (an initially unselected subset of FinnBrain Birth Cohort Study; Karlsson et al., 2017). DTI data acquisition was successful with 100 participants, and a complete DTI dataset was obtained from 85 participants. The final mean age of the participants was 5.3 years (standard deviation (SD) 0.75 months). The exclusion criteria in addition to general MRI contraindications included (1) Birth before gestational week 35 (based on the recommendation of neonatologist in the FinnBrain Birth Cohort study; before gestational week 32 for those with exposure to maternal prenatal synthetic glucocorticoid treatment), (2) major developmental disorder or trait (e.g. heart failure/surgery, missing limbs, major hereditary disorders, etc.), (3) other types of long-term diagnosis that requires constant contact to Hospital (autism, attention deficit disorder, epilepsy, etc.), (4) sensory abnormalities (e.g. blindness or deafness), (5) use of daily, regular medication (asthma inhalers with infections are common and were not used as an exclusion criteria; one exception with desmopressin [[®]Minirin] medication was allowed) and (6) head trauma requiring inpatient care (reported by parents). Apart from this, certain practical subject characteristics prevented participation, including ear tubes (recurrent otitis media treatment) or large dental braces.

2.2 | Study visits

Recruitment was carried out by two phone calls, after the first of which the family was provided time to consider their attendance and to confirm child assent. A careful preparation protocol was performed preceding each imaging visit to guarantee both the children's and parents' feelings of safety and comfort. This included a home visit by a study nurse providing more precise information concerning the visit and a home practice period to familiarise the participant with the feeling of immobilisation and the sounds of MRI scanner. During the home visit, a member of research staff was able to meet with the participating child and answer any remaining questions. The families were also encouraged to build home mock scanners for practice during home practice period (e.g. cardboard box with a hole for watching a movie through). We introduced the visit for the participants as a "space adventure" but were prepared to adjust the setting individually with children's own preferences. The

TABLE 1 Comparison of diffusion tensor imaging (DTI) scalar values, imaging parameters and analysis methods between the previous and present paediatric population studies

Study	Field strength (T)	Diffusion parameters	TR/TE (ms)	Pre-processing
		b0s b (s/mm ²) Directions		
Our study	3 T	12 1000 96	9300/87	<ul style="list-style-type: none"> • DTIprep • Eddy and motion correction • Tensor fitting (FSL)
(Rollins et al., 2010)	3 T	NA 700 30, 3 rep	9000/74	<ul style="list-style-type: none"> • Averaging with PRIDE • Eddy and motion correction • BET • Tensor fitting (FSL)
(Qiu et al., 2008)	3 T	1 1000 6, 4 rep	6000/84	<ul style="list-style-type: none"> • Eddy and motion correction • Tensor fitting (FSL)
(Krogsrud et al., 2016)	1.5 T	5 700 32	8200/81	<ul style="list-style-type: none"> • Eddy and motion correction • BET (FSL)
(Muftuler et al., 2012)	3 T	1 800 32	9290/55	<ul style="list-style-type: none"> • Eddy correction • Vector vs head motion correction (FSL) • BET • FDT (FSL)
(Colby et al., 2011)	1.5 T	1 1000 6, 3 rep	NA	<ul style="list-style-type: none"> • Eddy and motion correction • Tensor fitting (FSL)
(Swartz et al., 2015)	3 T	1 800 15, 2 rep	9000/82.3	<ul style="list-style-type: none"> • Eddy and motion correction • FDT • BET • dtifit (FSL)
(Seunarine et al., 2016)	1.5 T	1 1000 20, 3 rep	6300/89	<ul style="list-style-type: none"> • Eddy correction • BET (FSL)
(Moura et al., 2016)	1.5 T	NA 800 15, 2 rep	11,600/99	<ul style="list-style-type: none"> • FSL
(McGraw et al., 2002)	1.5 T	1 1,000 6, 2 rep	12,000/101	NA
(Hermoye et al., 2006)	1.5 T	1 700 32, 2 rep	7859/80	<ul style="list-style-type: none"> • DTI studio pre-processing
(Bonekamp et al., 2007)	1.5 T	2 1,000 15, 2 rep	NA/93.7	<ul style="list-style-type: none"> • Visual quality control for motion artefacts (DTIStudio) • Tensor fitting (DTIStudio, DTIPROC)

TABLE 1 (Continued)

Study	Field strength (T)	Diffusion parameters	TR/TE (ms)	Pre-processing
(Schmithorst et al., 2008)	3 T	3 710 25	6070/87	<ul style="list-style-type: none"> • BET (MRICro) • Eddy and field inhomogeneity correction • Tensor fitting (RESTORE) • Co-registration to WM probability map
(Tamnes et al., 2010)	1.5 T	10 700 30, 2 rep	8200/82	<ul style="list-style-type: none"> • Motion corrections • Eddy correction • Tensor fitting • FSL
(Loenneker et al., 2011)	3 T	5 1000 21	12,500/99.2	<ul style="list-style-type: none"> • Motion correction • Tensor fitting (diffusion toolbox, SPM5)
(Sadeghi et al., 2015)	1.5 T	4 1000/1100 6, 4 rep	9000/90 or 757,800/87	<ul style="list-style-type: none"> • TORTOISE pipeline • Eddy and motion corrections • RESTORE • tens • iR
(Genc et al., 2017)	3 T	7 1000/3000 61	6614/81 and 8112/104	<ul style="list-style-type: none"> • DTIprep QC • DTI-TK • FSL dtifit
(Moon et al., 2011)	3 T	1 1000 6, 4 rep	7200/90	<ul style="list-style-type: none"> • Matlab, custom made scripts • No eddy correction
(Taki et al., 2013)	3 T	1 1000 32	10,293/55	<ul style="list-style-type: none"> • Tensor fitting (software pre-installed on MR console (Philips) + SPM2 MATLAB)
(Chen et al., 2016)	1.5 T	NA 1000 6, 8 rep	6400/88	<ul style="list-style-type: none"> • Motion correction • Eddy correction • Tensor fitting (FSL) • DTI-TK for population-specific template + medial tract surface
(Lebel et al., 2016)	3 T	5 750 30	6750/79	<ul style="list-style-type: none"> • Motion and Eddy correction (in-house software) • Tensor fitting (FSL)
(Sarkar et al., 2014)	3 T	4 1300 32	TR varied between subjects/104.5	<ul style="list-style-type: none"> • Visual check for corruption • Motion and Eddy correction (explore-DTI), RESTORE
(Lebel et al., 2012)	1.5 T	NA 1000 6, 8 rep	6400/88	<ul style="list-style-type: none"> • Study specific template
(Wier et al., 2019)	3 T	NA 1000 32	10,000/60	<ul style="list-style-type: none"> • Data inspected for artefacts (method not mentioned)

TABLE 1 (Continued)

Study	Field strength (T)	Diffusion parameters	TR/TE (ms)	Pre-processing
(Scherf et al., 2014)	3 T	1 850 6, 12 rep	4900/82	<ul style="list-style-type: none"> DTISudio
(Tokariev et al., 2020)	3 T	3 1000 30	9000/80	<ul style="list-style-type: none"> TORTOISE, DTI-TK Eddy and motion correction
(Yu et al., 2020)	3 T	NA 1000 30, 2 rep	9300/100	<ul style="list-style-type: none"> DTISudio Eddy correction
(Young et al., 2019)	3 T	26 700/1000/2850 60	10,700/115 8800/87 10,700/115	<ul style="list-style-type: none"> FSL Eddy and motion correction RESTORE
(Hutton et al., 2020a, 2020b)	3 T	NA 2000 61	5000/88	<ul style="list-style-type: none"> FSL Eddy and motion correction Tensor fitting (FSL)
(Grohs et al., 2018)	3 T	5 750 30	6750/79	<ul style="list-style-type: none"> ExploreDTI Eddy and motion correction Manual motion detection
(Farah et al., 2020)	3 T	7 1000 61	8355/43	<ul style="list-style-type: none"> Vistalab diffusion MRI software Eddy and motion correction RESTORE
(Stephens et al., 2020)	3 T	7 1000 42	7680/82	<ul style="list-style-type: none"> DTIprep Eddy and motion correction
(Lee et al., 2019)	3 T	7 1000 42	7680/82	<ul style="list-style-type: none"> DTIprep Eddy and motion correction
(Reynolds et al., 2019)	3 T	5 750 30	6750/79	<ul style="list-style-type: none"> ExploreDTI

Note: Only examples of published scalar values are presented in the table. "Not reported, visualised in figure" is denoted if scalar values are reported only as a graph without exact values. Abbreviations: TR/TE = time of repetition/echo time, ms = milliseconds, rep = repetitions, TBSS = tract-based spatial statistics, ROI = region of interest, VBA = voxel-based analysis, FSL = FMRIB software library, BET = brain extraction tool, FDT = FMRIB's diffusion toolbox, y = year, mo = month, FA = fractional anisotropy, MD = mean diffusivity, RD = radial diffusivity, AD = axial diffusivity, WM = white matter, NA = not available, GCC = genu of corpus callosum, CC = corpus callosum, SCC = splenium of corpus callosum, CST = corticospinal tract, CG = cingulum, IC = internal capsule.

TABLE 1 (Continued)

Study	Analysis method	Age group N	FA	MD ($\times 10^{-3}$)	RD ($\times 10^{-3}$)	AD ($\times 10^{-3}$)
Our study	TBSS FA threshold 0.2	5.25–5.42 y N = 49				
(Rollins et al., 2010)	TBSS FA threshold 0.2	6–18 y N = 32	At age of 6 y GCC 0.88 SCC 0.85 CST 0.68–0.69 CG 0.38–0.55	NA	Not reported, visualised in figures	Not reported, visualised in figures
(Qiu et al., 2008)	TBSS, ROI (manual) FA threshold 0.2	Group 1: 6.8–7.9 y N = 24	GCC 0.87 SCC 0.88 IC 0.56–0.73	GCC 0.79 SCC 0.78 IC 0.81–0.84	GCC 0.23 SCC 0.22 IC 0.40–0.54	GCC 1.93 SCC 1.90 IC 1.46–1.73
(Krogsrud et al., 2016)	TBSS, ROI FA threshold 0.25	Time Point 1: 4.2–9.3 y 2: 5.8–11.9 y N = 159	Not reported, visualised in Figure 3 as change in FA vs age	Not reported, visualised in figure	Not reported, visualised in figure	Not reported, visualised in figure
(Muftuler et al., 2012)	TBSS	6–10 y N = 126	CST 0.54 CG 0.44	CST 0.76 CG 0.80	NA	NA
(Colby et al., 2011)	TBSS FA threshold 0.2, study specific template	5–28 y N = 32	Not reported, visualised in Figure 1	NA	Not reported, visualised in figure	Not reported, visualised in figure
(Swartz et al., 2015)	TBSS FA threshold 0.2	9.6–19.2 y N = 39	Not reported, visualised in Figure 1	NA	NA	NA
(Seunarine et al., 2016)	TBSS FA threshold 0.2	8–16.7 y N = 53	Not reported, visualised in Figure 4	Not reported, visualised in figure	Not reported, visualised in figure	Not reported, visualised in figure
(Moura et al., 2016)	TBSS, ROI	7–14 y N = 176	NA	NA	NA	NA
(McGraw et al., 2002)	ROI (Functool software)	36–71 mo N = 15	CC 0.784 IC 0.695	NA	NA	NA
(Hermoye et al., 2006)	ROI analysis (manual)	0–54 mo N = 30	No exact values of WM tracts, visualised in figure 4	Not reported, visualised in figure	NA	NA
(Bonekamp et al., 2007)	ROI analysis (manual)	5.5–19.1 y N = 44	GCC 0.75 CG 0.47	GCC 0.864 CG 0.708	NA	NA

TABLE 1 (Continued)

Study	Analysis method	Age group N	FA	MD ($\times 10^{-3}$)	RD ($\times 10^{-3}$)	AD ($\times 10^{-3}$)
(Schmithorst et al., 2008)	ROI analysis VBA	5–18 y N = 106 Age group < 10 y	Girls: SCC 0.80 Boys: SCC 0.72	Girls: CST 0.739 Boys: CST 0.766	NA	NA
(Tamnes et al., 2010)	ROI analysis, FA threshold 0.2	8–30 y N = 168	Not reported, visualised in figure 6	Not reported, visualised in figure 6	NA	NA
(Loenneker et al., 2011)	ROI Tractography threshold FA 0.2	5.4–7.8 N = 12	Not reported, visualised in Figure 1	Not reported, visualised in Figure 1	Not reported, visualised in Figure 1	Not reported, visualised in Figure 1
(Sadeghi et al., 2015)	ROI (manual)	4.1–22.2 y (values at age 4–5 y, reported as an intercept of scalar vs age plot)	GCC 0.86–0.88 CG 0.60 CST 0.72	GCC 0.74 CG 0.76 CST 0.87	NA	NA
(Genc et al., 2017)	ROI	4–19 y N = 72	Age 4–9.5 y CG 0.3–0.33 CST 0.49–0.5	NA	NA	NA
(Moon et al., 2011)	ROI (manual)	4.2–17.7 y N = 87	At age of 4–7 years GCC 0.53 SCC 0.62	ADC $\times 10^{-3}$ mm ² /s GCC 1.12 SCC 1.06	NA	NA
(Taki et al., 2013)	VBA, ROI analysis	5.6–18.4 y N = 246	NA	NA	NA	NA
(Chen et al., 2016)	FACT (DTIstudio) Surface along tracts for FA and MD values	6–30 y N = 178	Not reported, visualised in Figure 2	Not reported, visualised in Figure 2	NA	NA
(Lebel et al., 2016)	Tractography (TrackVis)	2.6–5.1 y N = 52	NA	Not reported, visualised in figure	Not reported, visualised in figure	Not reported, visualised in figure
(Sarkar et al., 2014)	Tractography (TrackVis)	6–9 y N = 22	Not reported, visualised in figure	NA	Not reported, visualised in figure	NA
(Lebel et al., 2012)	Tractography (ExploreDTI)	5–9 y N = 57	Not reported, equation fitted intercept values of reported in table	Not reported, equation fitted intercept values reported in table	NA	NA
(Wier et al., 2019)	Tractography (DSI studio) ROI (manual)	8–16 y N = 25 (healthy controls N = 14)	CG 0.49	CG 0.77–0.78	CG 0.54–0.56	CG 1.20–1.22

TABLE 1 (Continued)

Study	Analysis method	Age group N	FA	MD ($\times 10^{-3}$)	RD ($\times 10^{-3}$)	AD ($\times 10^{-3}$)
(Scherf et al., 2014)	Tractography ROI FACT	6–23 y N = 50	NA	Not reported, visualised in figure	Not reported, visualised in figure	Not reported, visualised in figure
(Tokariev et al., 2020)	TBSS FA threshold 0.2	7.6 y N = 16 controls + N = 16 preterm-born subjects	CC 0.8 CST 0.73–0.74	CC 0.88 CST 0.82	CC 0.31 CST 0.38–0.39	CC 2.04 CST 1.69
(Yu et al., 2020)	TBSS, FA threshold 0.2	0.17–7.91 y N = 118	Not reported, visualised in figure	Not reported	Not reported	Not reported
(Young et al., 2019)	TBSS, FA threshold 0.2	Mean 6.6 y N = 24 + N = 23 preterm-born subjects	Not reported	Not reported	Not reported	Not reported
(Hutton et al., 2020a, 2020b)	TBSS FA threshold 0.2	3–5.25 y N = 47	Not reported	Not reported	Not reported	Not reported
(Grohs et al., 2018)	Tractography	2.9–6.3 y N = 80	Not reported, visualised in figure	Not reported, visualised in figure	Not reported	Not reported
(Farah et al., 2020)	ROI Automatic fibre quantification	3.8 y N = 15 (only female)	CG 0.33–0.41	CG 0.83–0.86	Not reported	Not reported
(Stephens et al., 2020)	Tractography	0–6 y N = 146, 0 y N = 91, 1 y N = 62, 2 y N = 84, 4 y N = 94, 6 y	Average at 4y 0.415 Average at 6y 0.430	NA	Average at 4y 0.64 Average at 6y 0.61	Average at 4y 1.26 Average at 6y 1.25
(Lee et al., 2019)	Tractography	N = 215, 1 y N = 165, 2 y Twin-study	Not reported, visualised in figure	NA	Not reported, visualised in figure	Not reported, visualised in figure
(Reynolds et al., 2019)	Tractography	1.95–6.97 y N = 120	Predicted at 2y SCC 0.53 CG 0.39	Predicted at 2y SCC 0.91 GC 0.91	Predicted at 2y SCC 0.65 GC 0.71	Predicted at 2y SCC 1.54 GC 1.32

Note: Only examples of published scalar values are presented in the table. “Not reported, visualised in figure” is denoted if scalar values are reported only as a graph without exact values. Abbreviations: TR/TE = time of repetition/echo time, ms = milliseconds, rep = repetitions, TBSS = tract-based spatial statistics, ROI = region of interest, VBA = voxel-based analysis, FSL = FMRIB software library, BET = brain extraction tool, FDT = FMRIB’s diffusion toolbox, y = year, mo = month, FA = fractional anisotropy, MD = mean diffusivity, RD = radial diffusivity, AD = axial diffusivity, WM = white matter, NA = not available, GCC = genu of corpus callosum, CC = corpus callosum, SCC = splenium of corpus callosum, CST = corticospinal tract, CG = cingulum, IC = internal capsule.

imaging situation was simulated at the imaging centre with the aid of a wooden mock scanner head coil prior to scanning. Immobilisation was practised with the mock scanner and a toy brought by the participating child, and the effect of moving the toy during taking photos with a cell phone was demonstrated to indicate the importance of staying still during the scan.

The scans were performed awake or during natural sleep. The hearing protection was accomplished with a combination of ear plugs and earmuffs. The participants were able to watch a television programme of one's own choosing through a mirror system of the head coil during the image acquisition. Of note, although the movie watching may also increase sporadic motion, we noticed that it improved the overall compliance. The research staff was also able to communicate with the child through the headphones with which the audio was channelled through. One member of the research staff and a parent stayed in the scanner room, and the parent was able to touch the child's leg if the child wished this before the scan. A "signal ball" was given for the participant and throwing it in the case if he or she wanted to stop or pause was practised during training. The imaging was discontinued at any point if the child or the parent expressed unwillingness to continue. The total duration of the visit was approximately 3 h on average, and the maximum duration of the scanning protocol was 60 min.

All MRI images were reviewed by a neuroradiologist to detect any findings requiring further investigations, and a paediatric neurologist was consulted when necessary. An incidental finding requiring consultations was detected in one included case (1/110, 0.9%), and it was handled with our protocol described before (Kumpulainen et al., 2020). The finding did not affect the analysis of diffusion data.

2.3 | MRI data acquisition

The MRI scans were performed on a Siemens Magnetom Skyra fit 3 T scanner (Siemens Medical Solutions, Erlangen, Germany) using a 20-channel head/neck receiver coil at the Turku University Hospital. GeneRalised Autocalibrating Partially Parallel Acquisition was used to accelerate the image acquisition. The following sequences were acquired: T1-weighted sequence with time of repetition (TR)/time of echo (TE) = 1900/3.26 ms, field of view (FOV) 256 mm, voxel size $1.0 \times 1.0 \times 1.0$ mm and T2-weighted sequence (TR/TE = 6,400 ms/96.0 ms, FOV = 230 mm, voxel size $1.0 \times 1.0 \times 1.0$ mm). Diffusion weighted imaging protocol was applied with a standard twice-refocussed Spin Echo-Echo Planar Imaging (SE-EPI): TR/TE = 9300/87.0 ms,

FOV = 208 mm, isotropic voxels with $2.0 \times 2.0 \times 2.0$ mm resolution, b value 1000s/mm² and 96 noncollinear diffusion gradient directions divided into three scanning sets (31, 32 and 33 directions) with 9 b_0 images (3 $b_0 = 0$ s/mm² volumes scattered within each set). Additionally, multi-shell data including b values 650 and 2000 s/mm² were acquired from part of the participants ($n = 70$) with the following setting: (1) TR/TE = 5000/79.0 ms, FOV = 208 mm, isotropic voxels with $2.0 \times 2.0 \times 2.0$ mm resolution, b value 650 s/mm², 34 noncollinear diffusion gradient directions and 4 b_0 images, and (2) TR/TE = 5000/114 ms, FOV = 208 mm, isotropic voxels with $2.0 \times 2.0 \times 2.0$ mm resolution, b value 2000s/mm², 80 noncollinear diffusion gradient directions and 10 b_0 images divided into two scanning sets. Only data with b value 1000s/mm² were used in this substudy. We chose DTI protocol with b value 1000s/mm² for our evaluations because of common use of 1000 s/mm² b value in the literature, and because all subjects of our study cohort contained data with that protocol. DTI sequences were divided into shorter sets. This permitted to take breaks during scanning protocol if required. Repetition of individual sequence was also possible if major corruption of images was detected immediately during the scan.

2.4 | Image analysis

The data were converted to NIFTI format and pre-processed using FSL 6.0 software (FMRIB software library, University of Oxford, UK). We chose not to perform distortion corrections, which is a frequently performed pre-processing step for contemporary analyses. We found out that for some of the scans, field maps were corrupted, and because our scans did not suffer from major distortions before corrections, we opted to leave this step out of the pipeline—we do not consider this to alter the result. b_0 images were reviewed by visual quality control, and images with insufficient quality were manually excluded. Examples of b_0 and diffusion volumes prior to the pre-processing are provided in the supporting information (Figure S1). Passed b_0 images that included at least one image per imaging set were co-registered and averaged (FMRIB's Linear Image Registration Tool) and used to create a brain mask using Brain Extraction Tool (BET version 1.0.0) (Smith, 2002) with settings -R -f 0.3 (with three exceptions of -f 0.2 because of problems with brain borderline recognition). Quality of the diffusion volumes was controlled using DTIprep (<https://nitrc.org/projects/dtiprep/>) [Oguz et al., 2014] version 1.1.0) with default settings. We chose rather to include the volumes with acceptable quality than to optimise the DTIprep

sensitivity in detecting motion artefacts in expense of decreasing specificity and thus missing volumes. During quality control, DTIprep was detected to retain many directions with severe corruptions with these settings. The passed diffusion gradients were quality controlled visually (by VK), and directions corrupted with artefacts were manually excluded in addition to directions discarded by DTIprep. Motion and eddy current correction were performed with FSL tools with concurrent rotation of the directional vectors (.bvec file). Forty-nine participants were included into the subsequent analysis (subjects with at least 66 directions after quality control steps; 21 females), whereas others needed to be excluded owing to loss of over 30 directions because of movement-corruption, to obtain minimum of 66 directions for each subject for the subsequent analysis (success rate with this choice 49/110, 45% of subjects attending the MRI visit; 49/85, 58% of subjects who completed the whole DTI data acquisition), see Figure 1 flow chart of the study population. It must be noted that the criteria we set for exclusion resulted in 55% data loss for the analyses of the current study, but we felt it was necessary to form an ideal data for our research questions. On a related note, the success rates for all the scans we performed are much higher, for example, for participants having at least 40 quality-controlled diffusion-encoding directions were 84% (147/173) in the full sample.

Subsets including variable numbers of diffusion gradient directions ($N = 6, 9, 12, 15, 18, 24, 30, 36, 42, 48, 54, 60, 66$) were formed by rejecting directions in a way that maximised the final angular resolution calculated with the spherical Voronoi algorithm in the SciPy python library (Caroli et al., 2010; Millman & Aivazis, 2011). DTI fitting was performed with FSL's dtifit to compute scalar maps (FA, MD, RD and AD).

Subsequently, the Tract-Based Spatial Statistics (TBSS) pipeline of FSL (Smith et al., 2006) was used to estimate WM tract skeletons separately for each subset. TBSS method utilises nonlinear alignment of targets relieving problems of voxel-based analyses concerning imperfect brain-to-brain alignment and spatial smoothing. The most representative FA image among the subset was chosen as a target image, followed by nonlinear transformation and affine registration of every other image to the target ("tbss_2_reg" flag -n). Of note, the use of -n flag for tbss_2_reg means that the process will: "... align every FA image to every other one, identify the 'most representative' one, and use this as the target image. This target image is then affine-aligned into MNI152 (Montreal Neurological Institute) standard space, and every image is transformed into $1 \times 1 \times 1$ mm MNI152 space by combining the nonlinear transform to the target FA image with the affine transform from that

Study population attending
the imaging visits
n = 110



DTI data gathered
n = 100



complete set of 96
directions before
quality control
n = 85

66 directions after quality control
n = 49

FIGURE 1 Flow chart of the study population

target to MNI152 space ...", that is, the template is study specific. We have also supplied representative images over the warp fields used to perform the co-registration (supporting information Figure S2) to demonstrate the alignment of the data. The alignment between the target and the MNI 152 standard space was further visually inspected for detection of alignment errors in the peripheral regions. The mean FA skeleton across the subjects was formed, and this study-specific template was applied to create FA skeletons using typically applied FA threshold value 0.2. In addition, the effect of FA threshold value was assessed by repeating the statistical analysis later with TBSS skeleton calculated with threshold values 0.1, 0.125, 0.15, 0.175 and 0.3 to estimate the effect of different thresholds. Other scalar maps of MD, AD and RD were co-registered on the mean FA image by using "tbss_non_FA" script.

In region of interest (ROI) analysis, WM tracts were defined by aligning the scalar maps to JHU-ICBM-DTI-81 WM atlas (Mori et al., 2008; Oishi et al., 2008). JHU ROIs were calculated for each subject in skeleton space, corresponding to the skeletonised study-specific template space. Part of the atlas WM tracts were misaligned or not present in the field of view in our MRI data (the cerebellum was not included in our field of view) and were thus disregarded. The incorporated WM tracts are splenium, body and genu of corpus callosum (SCC, BCC, GCC), fornix and bilateral corticospinal tract (CST), anterior and

posterior limbs of internal capsule (ALIC, PLIC), superior longitudinal fasciculus (SLF), superior fronto-occipital fasciculus (SFOF), inferior longitudinal fasciculus/inferior fronto-occipital fasciculus (ILF/IFOF), cingulate gyrus (CG), cingulum (CING), uncinate fasciculus (UNC), anterior/superior/posterior corona radiata (ACR, SCR, PCR), retrolenticular internal capsule (rl IC), external capsule (EC), posterior thalamic radiation including optic tract (PTR/OT) and cerebral peduncle (CP). Mean scalar values of voxels in each tract for each subject were extracted separately for both skeletonised and non-skeletonised overall WM area resulting in 38 ROIs.

Rotation and transformation because of motion during image acquisition were estimated from eddy-motion correction parameters to control the effect of minor residual motion. Motion statistics were derived after both DTIprep and manual exclusion of motion corrupted volumes, in a procedure described in more detail in our previous study (Merisaari et al., 2019). Values observing the head displacement exclusively in respect of the previous scanned direction were used to assess separately the amount of abundant back and forth movement as well as extensive total head displacement.

2.5 | Statistical analysis

Statistical analyses were performed with Rstudio (version 1.3.1093). For each scalar value (FA, MD, RD and AD), the mean, median, kurtosis and skewness were calculated in each WM tract ROI with the number of directions as a variable. Both skeletonised and scalar values within the entire WM ROI were separately inspected to detect the effect of using the TBSS skeleton. Statistically significant differences between datasets were estimated by one-way analysis of variance (ANOVA) test, and if significant, followed by a Tukey test to detect group-wise difference. False discovery rate correction was applied and thresholded at $p < 0.01$. We performed the statistical tests also with median values that reduce the significance of extreme values (misplacement of borderline voxels because of inaccuracies in atlas alignment). Intraclass correlation coefficient (ICC) (Shrout & Fleiss, 1979) was calculated with two-way random-effects model (ICC[2,1]) to assess the repeatability of results with different amount of diffusion-encoding directions. The number of diffusion directions were considered as raters. The following sets were formed over of which the ICC analysis was performed: (1) N6-to-N66 (including subsets of all permuted amounts of directions between N6 and N66), (2) N12-to-N66 (including subsets N12 to N66), (3) N18-to-N66 (including subsets N18 to N66) and

(4) N24-to-N66 (including subsets N24 to N66). The effect of FA threshold on the results was estimated by multiple regression by defining interaction of number-of-direction*threshold. Motion statistics were calculated from motion between consecutive volumes to exclude the information on direction of the motion. Mean absolute motion in each direction (rotation and translation in x, y and z axis) was calculated by subjects, and the correlation between each WM tract FA value and motion was computed. As motion statistics were not normally distributed according to Shapiro–Wilk test, Spearman rank correlation was used. The correlation analyses were conducted with Statistical Package for the Social Sciences version 27.0 (IBM Corp. 2020, Armonk, NY, USA). The python codes that were used to analyse the data are available at <https://hub.docker.com/r/haanme/dtipipeline>, and R codes are provided at the end of the supporting information.

3 | RESULTS

A significant effect of the number of diffusion-encoding gradient directions on resultant DTI indices was detected in all WM tracts examined. Especially FA (Figure 2), RD and AD (Figure 3) depended on the number of diffusion directions, whereas the effect on MD (Figure 3) was less prominent and not present in all WM tracts. The corresponding figures of scalar values in other WM tract ROIs (TBSS skeleton ROIs for MD, RD and AD and entire WM tract ROIs (non-skeletonised) for FA) are presented in the supporting information (Figures S3–S6).

3.1 | DTI scalar values with 66 directions

Scalar values (FA and MD) for separate WM tracts with 66 diffusion-encoding directions in both TBSS skeleton ROIs and entire WM tract ROIs are shown in Table 2. The corresponding values for RD and AD are presented in supporting information Table S7.

3.2 | The effect of number of directions on DTI scalar values

Decreasing the number of diffusion-encoding directions deteriorated the accuracy and increased the variance of resultant scalar values. The scalar values in all TBSS ROIs showed inconsistent results with less than 18 directions without a direct trend (Figure 2, Tables 3 and 4). Increasing the number of directions to 18 or over resulted in consistent values with statistically significant differences

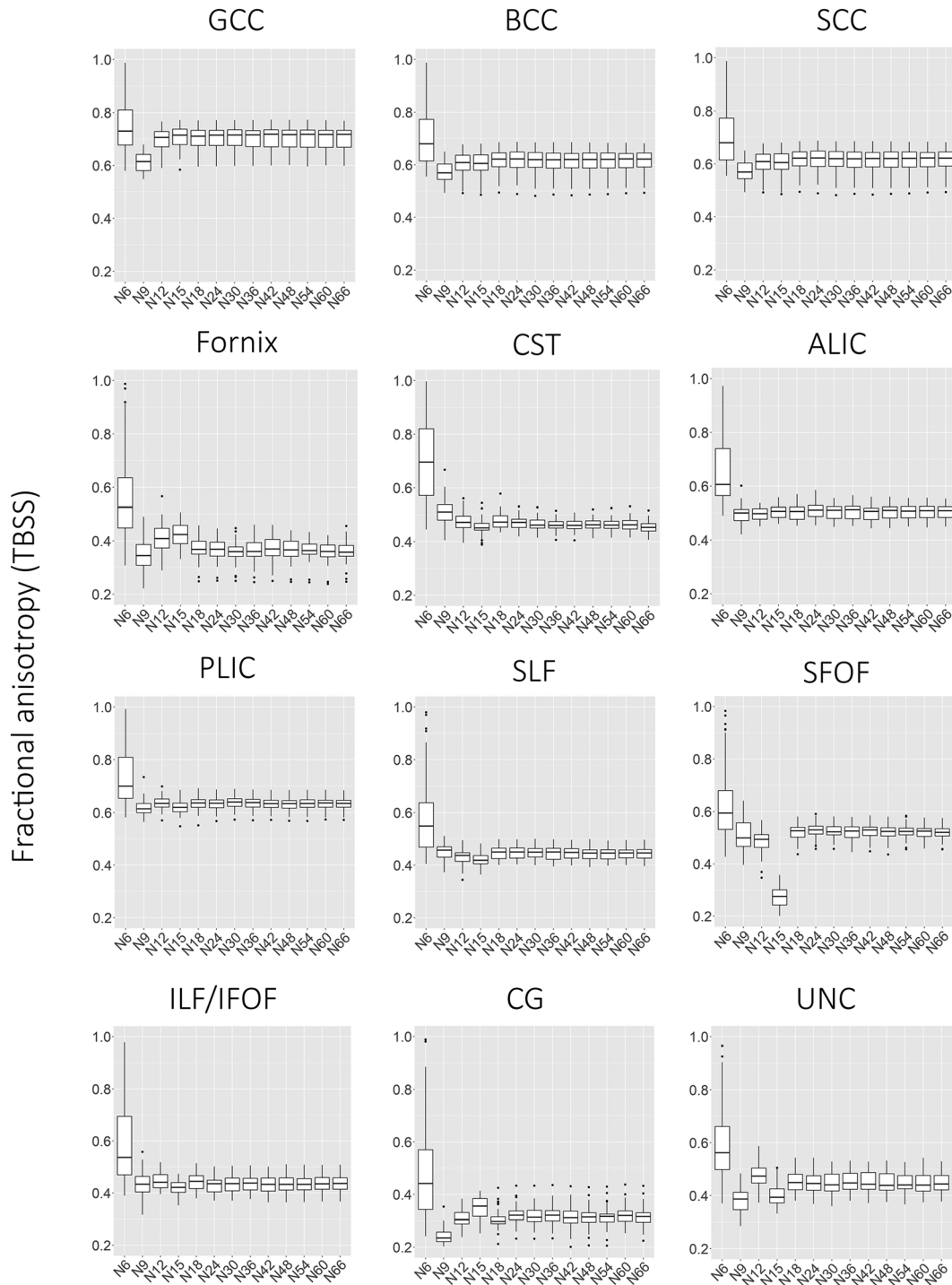


FIGURE 2 Mean fractional anisotropy values of selected white matter tract regions of interest TBSS (tract-based spatial statistics) skeleton voxels, plotted with separate number of diffusion-encoding directions (6, 9, 12, 15, 18, 24, 30, 36, 42, 48, 54, 60, 66). GCC = genu of corpus callosum, BCC = body of corpus callosum, SCC = splenium of corpus callosum, CST = corticospinal tract, ALIC = anterior limb of internal capsule, PLIC = posterior limb of internal capsule, SLF = superior longitudinal fasciculus, SFOF = superior fronto-occipital fasciculus, ILF/IFOF = inferior longitudinal fasciculus and inferior fronto-occipital fasciculus (sagittal stratum), CG = cingulate gyrus, UNC = uncinata fasciculus. With bilateral tracts, the right tract is demonstrated in the figure

detected in none of the WM tracts between direction numbers of 18 and 66 with TBSS (ANOVA $p > 0.01$; supporting information Table S8A and Figures 2 and 3).

Similar results were detected with entire WM tract ROIs (non-skeletonised data, supporting information S3 and S8B). The use of median values in statistical analyses had

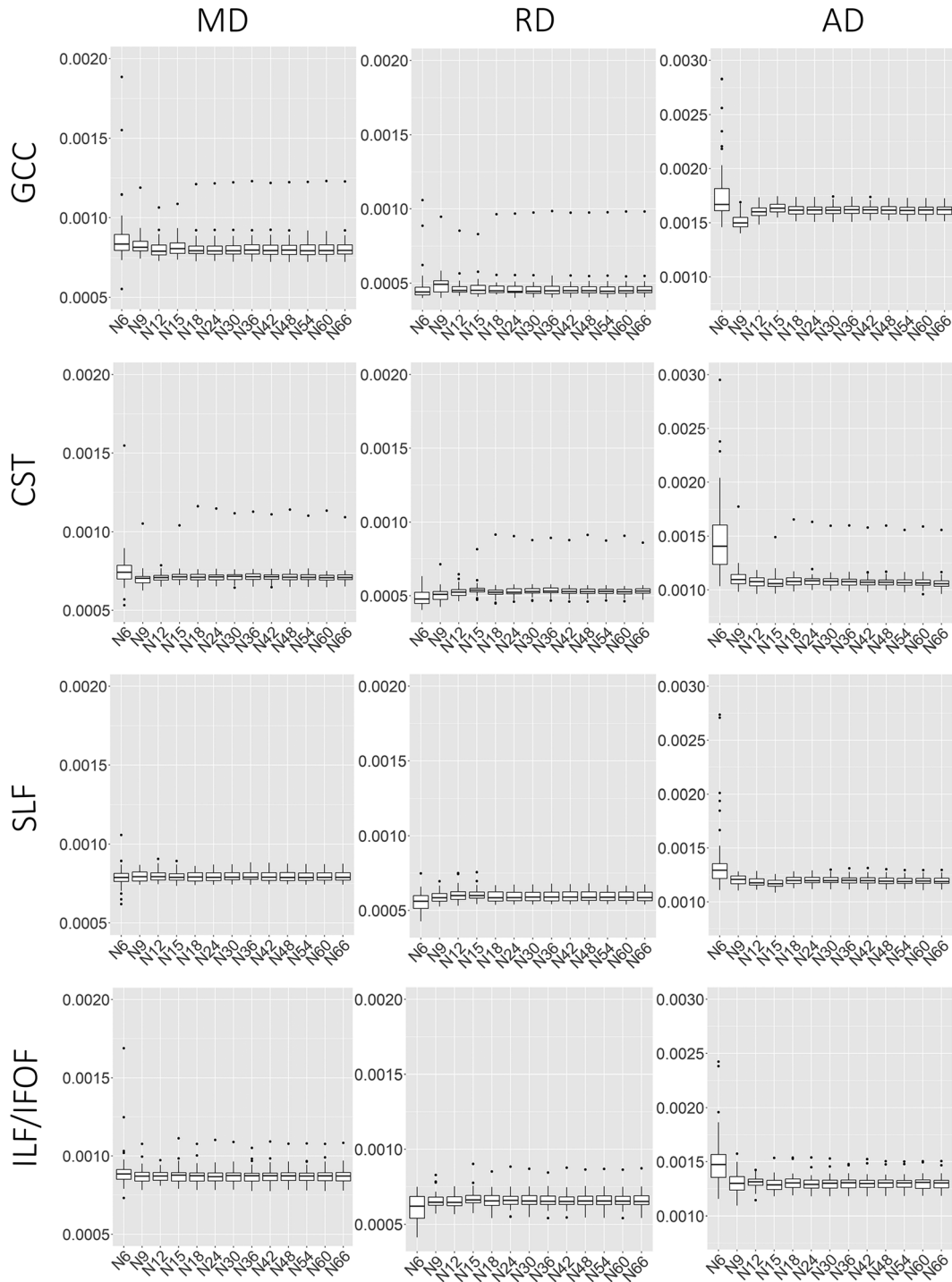


FIGURE 3 MD (mean diffusivity), RD (radial diffusivity) and AD (axial diffusivity) values of selected white matter tract regions of interest TBSS (tract-based spatial statistics) skeleton voxels plotted with separate number of diffusion-encoding directions. GCC = genu of corpus callosum, CST = corticospinal tract, SLF = superior longitudinal fasciculus, ILF/IFOF = inferior longitudinal fasciculus/inferior fronto-occipital fasciculus. With bilateral tracts, the right tract is demonstrated in the figure

no significant effect on the results within subsets N18 onwards (supporting information Figure S9, showing examples of GCC, CG and ALIC).

Fluctuation between overestimation and underestimation of values in low direction numbers (6 to

15 directions) was detected (Figure 2). The fluctuation existed especially in minor tracts, and also in the cingulum bundle, generally kept as one of the major WM tracts, which showed significant fluctuation of scalar values with low number of directions.

TABLE 2 Scalar values in white tracts as mean values across the entire tract voxels and TBSS (tract-based spatial statistics) skeleton voxels with 66 diffusion-encoding directions

	FA		MD	
	All voxels (mean ± SD)	Skeleton voxels (mean ± SD)	All voxels (mean ± SD × 10 ⁻³)	Skeleton voxels (mean ± SD × 10 ⁻³)
GCC	0,50 ± 0,029	0,70 ± 0,040	0,97 ± 0,069	0,81 ± 0,076
BCC	0,43 ± 0,027	0,61 ± 0,042	0,95 ± 0,043	0,88 ± 0,051
SCC	0,46 ± 0,022	0,70 ± 0,029	0,89 ± 0,028	0,80 ± 0,038
CST R	0,41 ± 0,019	0,45 ± 0,022	0,76 ± 0,056	0,72 ± 0,060
CST L	0,42 ± 0,020	0,47 ± 0,022	0,75 ± 0,023	0,70 ± 0,023
ALIC R	0,34 ± 0,019	0,50 ± 0,028	0,76 ± 0,024	0,76 ± 0,027
ALIC L	0,39 ± 0,020	0,48 ± 0,026	0,77 ± 0,030	0,76 ± 0,031
PLIC R	0,51 ± 0,020	0,63 ± 0,023	0,77 ± 0,022	0,77 ± 0,020
PLIC L	0,52 ± 0,021	0,65 ± 0,024	0,77 ± 0,046	0,76 ± 0,045
CG R	0,22 ± 0,021	0,32 ± 0,042	0,88 ± 0,050	0,84 ± 0,060
CG L	0,23 ± 0,022	0,46 ± 0,053	0,88 ± 0,044	0,84 ± 0,089
SLF R	0,37 ± 0,020	0,44 ± 0,024	0,79 ± 0,034	0,79 ± 0,032
SLF L	0,36 ± 0,020	0,44 ± 0,027	0,79 ± 0,027	0,80 ± 0,028
SFOF R	0,46 ± 0,034	0,52 ± 0,028	0,73 ± 0,028	0,73 ± 0,021
SFOF L	0,40 ± 0,036	0,50 ± 0,035	0,77 ± 0,095	0,73 ± 0,081
UNC R	0,33 ± 0,031	0,45 ± 0,038	0,89 ± 0,027	0,82 ± 0,028
UNC L	0,35 ± 0,029	0,44 ± 0,039	0,88 ± 0,021	0,84 ± 0,030
Fornix	0,32 ± 0,031	0,36 ± 0,041	1,61 ± 0,166	1,46 ± 0,187
CP R	0,44 ± 0,022	0,60 ± 0,028	1,11 ± 0,051	0,85 ± 0,071
CP L	0,46 ± 0,023	0,62 ± 0,029	1,09 ± 0,048	0,82 ± 0,042
IC R	0,46 ± 0,022	0,51 ± 0,026	0,87 ± 0,072	0,86 ± 0,061
IC L	0,48 ± 0,021	0,53 ± 0,024	0,85 ± 0,069	0,86 ± 0,072
ACR R	0,38 ± 0,026	0,44 ± 0,028	0,85 ± 0,037	0,81 ± 0,035
ACR L	0,38 ± 0,027	0,45 ± 0,029	0,85 ± 0,048	0,81 ± 0,042
SCR R	0,40 ± 0,021	0,45 ± 0,025	0,78 ± 0,024	0,78 ± 0,024
SCR L	0,41 ± 0,020	0,47 ± 0,022	0,80 ± 0,030	0,79 ± 0,029
PCR R	0,36 ± 0,024	0,41 ± 0,030	0,90 ± 0,038	0,90 ± 0,042
PCR L	0,38 ± 0,022	0,42 ± 0,027	0,91 ± 0,047	0,89 ± 0,041
PTR/OR R	0,44 ± 0,027	0,53 ± 0,034	0,95 ± 0,085	0,91 ± 0,060
PTR/OR L	0,43 ± 0,026	0,51 ± 0,035	0,96 ± 0,076	0,90 ± 0,048
ILF/IFOF R	0,39 ± 0,028	0,43 ± 0,033	0,88 ± 0,047	0,87 ± 0,049
ILF/IFOF L	0,37 ± 0,025	0,46 ± 0,029	0,88 ± 0,063	0,87 ± 0,042
EC R	0,31 ± 0,018	0,37 ± 0,023	0,82 ± 0,024	0,81 ± 0,026
EC L	0,33 ± 0,019	0,39 ± 0,025	0,80 ± 0,020	0,81 ± 0,025
CING R	0,23 ± 0,019	0,33 ± 0,037	0,86 ± 0,036	0,85 ± 0,041
CING L	0,23 ± 0,023	0,36 ± 0,041	0,90 ± 0,059	0,85 ± 0,032
Fornix/ST R	0,34 ± 0,022	0,47 ± 0,031	1,05 ± 0,090	0,93 ± 0,085
Fornix/ST L	0,35 ± 0,023	0,53 ± 0,036	1,03 ± 0,087	0,87 ± 0,070

Note: FA = fractional anisotropy, MD = mean diffusivity, GCC = genu of corpus callosum, BCC = body of corpus callosum, SCC = splenium of corpus callosum, CST = corticospinal tract, R = right, L = left, ALIC = anterior limb of internal capsule, PLIC = posterior limb of internal capsule, CG = cingulate gyrus, SLF = superior longitudinal fasciculus, SFOF = superior fronto-occipital fasciculus, UNC = uncinate fasciculus, CP = cerebral peduncle, IC = internal capsule (retrolenticular part), ACR = anterior corona radiata, SCR = superior corona radiata, PCR = posterior corona radiata, PTR/OR = posterior thalamic radiation/optic radiation, ILF/IFOF = inferior longitudinal fasciculus and inferior fronto-occipital fasciculus (sagittal stratum), EC = external capsule, CING = cingulum (hippocampus), ST = stria terminalis

TABLE 3 Mean FA (fractional anisotropy) values of whole white matter tract (all voxels) or TBSS (tract-based spatial statistics) skeleton voxels (skeleton voxels) with 66, 18 or 6 diffusion-encoding directions

	N66			N18			N6		
	All voxels (mean ± SD)	Skeleton voxels (mean ± SD)	Cohen's d	All voxels (mean ± SD)	Skeleton voxels (mean ± SD)	Cohen's d	All voxels (mean ± SD)	Skeleton voxels (mean ± SD)	Cohen's d
GCC	0,50 ± 0,029	0,70 ± 0,040	-	0,51 ± 0,028	0,70 ± 0,039	-	0,65 ± 0,14	0,75 ± 0,10	0,66
BCC	0,43 ± 0,027	0,61 ± 0,042	-	0,44 ± 0,027	0,61 ± 0,042	-	0,62 ± 0,15	0,71 ± 0,12	1,11
SCC	0,46 ± 0,022	0,70 ± 0,029	-	0,47 ± 0,022	0,70 ± 0,031	-	0,62 ± 0,16	0,67 ± 0,14	0,30
CST R	0,41 ± 0,019	0,45 ± 0,022	0,12	0,43 ± 0,025	0,48 ± 0,028	0,12	0,69 ± 0,17	0,72 ± 0,16	2,36
ALIC R	0,34 ± 0,019	0,50 ± 0,028	-	0,33 ± 0,019	0,50 ± 0,028	-	0,62 ± 0,16	0,66 ± 0,14	1,58
PLIC R	0,51 ± 0,020	0,63 ± 0,023	-	0,50 ± 0,020	0,63 ± 0,024	-	0,69 ± 0,13	0,74 ± 0,11	1,38
CG R	0,22 ± 0,021	0,32 ± 0,042	0,049	0,23 ± 0,022	0,30 ± 0,039	0,049	0,48 ± 0,19	0,50 ± 0,19	1,31
SLF R	0,37 ± 0,020	0,44 ± 0,024	0,41	0,37 ± 0,020	0,45 ± 0,025	0,41	0,56 ± 0,19	0,59 ± 0,16	1,31
SFOF R	0,46 ± 0,034	0,52 ± 0,028	-	0,47 ± 0,035	0,52 ± 0,031	-	0,60 ± 0,16	0,63 ± 0,16	0,96
UNC R	0,33 ± 0,031	0,45 ± 0,038	-	0,34 ± 0,033	0,45 ± 0,039	-	0,58 ± 0,16	0,60 ± 0,16	1,29
Fornix	0,32 ± 0,031	0,36 ± 0,041	0,25	0,32 ± 0,033	0,37 ± 0,040	0,25	0,56 ± 0,17	0,57 ± 0,17	1,70
PTR/OR R	0,44 ± 0,027	0,53 ± 0,034	-	0,45 ± 0,027	0,53 ± 0,032	-	0,58 ± 0,17	0,64 ± 0,14	1,08
ILF/IFOF R	0,39 ± 0,028	0,43 ± 0,033	0,31	0,39 ± 0,027	0,44 ± 0,032	0,31	0,56 ± 0,18	0,60 ± 0,17	1,39
CING R	0,23 ± 0,019	0,33 ± 0,037	0,29	0,24 ± 0,020	0,32 ± 0,032	0,29	0,54 ± 0,20	0,55 ± 0,20	1,53
Fornix/ST R	0,34 ± 0,022	0,47 ± 0,031	0,30	0,34 ± 0,022	0,48 ± 0,035	0,30	0,59 ± 0,18	0,62 ± 0,17	1,23

Note: Effect sizes calculated with Cohen's *d* are in relation to TBSS N66, using average of SD (standard deviation) values. GCC = genu of corpus callosum, BCC = body of corpus callosum, SCC = splenium of corpus callosum, CST R = right corticospinal tract, ALIC R = right anterior limb of corona radiata, PLIC R = posterior limb of corona radiata, CG R = right cingulum, SLF R = right superior longitudinal fasciculus, SFOF R = right superior fronto-occipital fasciculus, UNC R = right uncinate, PTR/OR R = right posterior thalamic radiation/optic tract, ILF/IFOF R = right inferior longitudinal fasciculus/inferior fronto-occipital fasciculus, CING R = right cingulate gyrus, ST R = right stria terminalis.

TABLE 4 Intraclass correlation coefficients (ICC) and 95% confidence intervals (CI) for FA (fractional anisotropy) values of the entire white matter tract region of interest voxels or TBSS (tract-based spatial statistics) skeleton region of interest voxels across groups including the following direction subsets: (1) N6-to-N66, (2) N12-to-N66, (3) N18-to-N66 and (4) N24-to-N66

FA								
	N6-to-N66 [CI]		N12-to-N66 [CI]		N18-to-N66 [CI]		N24-to-N66 [CI]	
GCC	0.305	[0.215;0.425]	0.975	[0.964;0.984]	0.993	[0.990;0.996]	0.996	[0.994;0.998]
SCC	0.148	[0.0862;0.242]	0.948	[0.925;0.967]	0.994	[0.986;0.994]	0.991	[0.987;0.995]
CST R	0.109	[0.0557;0.192]	0.764	[0.684;0.838]	0.882	[0.835;0.923]	0.906	[0.866;0.939]
ALIC R	0.136	[0.0762;0.226]	0.935	[0.907;0.958]	0.962	[0.945;0.976]	0.974	[0.962;0.984]
PLIC R	0.165	[0.0996;0.263]	0.936	[0.908;0.958]	0.978	[0.968;0.986]	0.985	[0.977;0.990]
CG R	0.0958	[0.0456;0.175]	0.768	[0.689;0.841]	0.912	[0.875;0.943]	0.925	[0.892;0.951]
SLF R	0.127	[0.0692;0.215]	0.947	[0.923;0.966]	0.976	[0.965;0.985]	0.983	[0.974;0.989]
SFOF R	0.292	[0.204;0.411]	0.875	[0.826;0.918]	0.975	[0.963;0.984]	0.982	[0.974;0.989]
FA skeleton								
	N6-to-N66 [CI]		N12-to-N66 [CI]		N18-to-N66 [CI]		N24-to-N66 [CI]	
GCC	0.639	[0.542;0.740]	0.989	[0.983;0.993]	0.995	[0.993;0.997]	0.997	[0.995;0.998]
SCC	0.302	[0.213;0.421]	0.966	[0.951;0.978]	0.990	[0.985;0.993]	0.991	[0.987;0.994]
CST R	0.136	[0.0767;0.227]	0.742	[0.658;0.822]	0.868	[0.815;0.913]	0.904	[0.863;0.938]
ALIC R	0.288	[0.201;0.407]	0.949	[0.927;0.968]	0.973	[0.960;0.983]	0.978	[0.968;0.986]
PLIC R	0.306	[0.217;0.426]	0.957	[0.937;0.972]	0.976	[0.966;0.985]	0.982	[0.974;0.989]
CG R	0.225	[0.148;0.335]	0.864	[0.811;0.910]	0.944	[0.920;0.964]	0.954	[0.933;0.971]
SLF R	0.197	[0.125;0.302]	0.928	[0.897;0.953]	0.972	[0.959;0.982]	0.978	[0.968;0.986]
SFOF R	0.245	[0.1640.358]	0.691	[0.598;0.782]	0.954	[0.934;0.971]	0.961	[0.943;0.975]

GCC = genu of corpus callosum, SCC = splenium of corpus callosum, CST R = right corticospinal tract, ALIC R = right anterior limb of corona radiata, PLIC R = posterior limb of corona radiata, CG R = right cingulum, SLF R = right superior longitudinal fasciculus, SFOF R = right superior fronto-occipital fasciculus.

In corpus callosum, mean FA of TBSS skeleton ranged from 0.67–0.75 (SD 0.10–0.14) in subset of six directions to 0.61–0.70 (SD 0.029–0.040) in subset of 66 directions (regarded as a standard in this study). The greatest effect of the number of directions on FA values was detected in CST with skeleton values ranging between 0.46 (with N66) and 0.72 (with N6). Differences between FA values achieved by using 6, 18 or 66 directions including effect sizes with and without applying TBSS skeleton are demonstrated in Table 3.

The MD values were less affected by the number of diffusion directions, and in part of the WM tracts statistically significant difference were not detected between subsets of 6 to 18 directions (p values ranging from 0.99 to < 0.01) (Figure 3).

Non-skeletonised FA values including all tract voxels showed greater degree of dependence on the number of directions used in the analysis (supporting information Figure S3). TBSS was indicated to reduce but not to completely remove the distortions of values caused by

low number of directions (Figure 2 and supporting information Figures S3 and S9). TBSS decreased the bias of FA values caused by low number of directions in areas of higher FA values (CC and CST) but conversely was detected to increase the fluctuation of values in lower FA areas (CG, ILF/IFOF and SFOF). In the subset of six directions, the variance of FA values correlated negatively with the FA value of the tract ($r = -0.83$, $p < 0.0001$), whereas with 66 directions, the FA value was not correlated with the variance ($r = 0.12$, $p = 0.46$).

Increasing the FA threshold to 0.3 had no significant effect on the results or changes to the minimum number of directions required (supporting information Figure S9). In areas with low FA values (for example, CG with voxels of FA values under 0.3) using threshold 0.3 increased the variation compared to values with FA threshold 0.2. The effect of using lower FA thresholds was also estimated and resulted in no significant effect with number-of-direction*threshold interaction (supporting information S10; also TBSS skeleton with thresholds

0.10, 0.15 and 0.20 presented). Of note, the TBSS skeletons with thresholds 0.10 and 0.15 extended to the grey matter in multiple areas.

3.3 | Intraclass correlation coefficient

Intraclass correlation coefficient (ICC[2,1]) analyses showed high repeatability of results with at least 18 directions (results for FA values are presented in Table 4). Within groups including subsets N6 to N15, the results showed low intraclass correlation (ICC range from 0.0958 to 0.639 with N6-to-N66), whereas groups with at least 18 directions (N18-to-N66 and N24-to-N66) presented with highly uniform results, with the ICC values in the examined TBSS WM tracts ranging between 0.868–0.995 and 0.904–0.997, respectively. Significant difference between groups N18-to-N66 and N24-to-N66 was not detected (95% confidence intervals of ICC values were overlapping). ICC calculated with MD values showed higher correlation within subsets of lower number of directions (for N6-to-N66 0.274 to 0.633 for all WM tract voxels and 0.154 to 0.689 for TBSS skeleton voxels) (supporting information Table S11), implying the lesser effect of the number of directions on the absolute MD values. Even though, similarly remarkably higher intraclass correlations were observed within subsets of more diffusion directions (for N18-to-N66 ranging between 0.963 and 0.998).

3.4 | The effects of within-scan motion on scalar values

Minor residual rotational and translational head movements were detected after motion correction protocol with no significant effect on the resultant DTI scalar values. The overall mean and maximum within-scan head motion values are demonstrated in supporting information Table S12. The estimated mean displacement between volumes remained low with values of translational movement ranging between 0.36 and 0.91 (\pm 0.16–0.26) mm and rotational movement between 0.13 and 0.20 (\pm 0.067–0.010) degrees. Excessive mean head motion of over a voxel size (2 mm) was detected in none of the subjects in none of the axes. The head displacement was not detected to correlate with DTI scalar values (supporting information Table S13) with exception of correlation between fornix and rotational movement exceeding statistical significance. The analysis was repeated for FA values with six directions resulting no significant correlations.

4 | DISCUSSION

We formed a simulated dataset where we experimentally altered the number of diffusion-encoding directions between 66 and 6. The ICC values were consistently high in datasets with more than 18 diffusion-encoding directions analysed with TBSS. These results indicate that a minimum of 18 directions is required for repeatable DTI scalar values. A similar trend was observed for ROI data outside the skeletonised dataset. Following exclusion of motion-corrupted volumes with DTIprep and manual quality control, minor residual motion did not associate with the scalar values. We established these conclusions in a sample of DTI data collected from healthy 5-year-old children with a narrow age range, which fills a gap in normative and methodological aspects of the field.

4.1 | DTI scalar values

Developmental changes in WM tract characteristics have commonly been reported in several studies to involve widespread increases in FA and decreases in MD values (Lebel & Deoni, 2018). Despite parallel developmental results, the variation in DTI scalar values of specified WM tracts between studies is wide. We reported the scalar values, and they seemed to fall within typical range (Table 1), although ROI scalar values have not been systematically reported in prior studies.

In this sample, TBSS FA values ranged between 0.7 in GCC and SCC, and 0.32 in right CG, which are included in the range of previously reported FA values in young children (Table 1). Tract-specific FA values are rarely reported and mostly offered as part of linear graphs without exact values, which reduces data transparency and complicates the comparison of results and evaluation of data quality. For example, out of all studies included in our literature review, only 13/33 (see Table 1) reported explicit DTI scalar values per chosen WM tracts. In these reviewed studies, DTI scalar values among paediatric populations vary substantially. Most frequently reported WM tracts are corpus callosum and corticospinal tracts, in which the reported TBSS FA values in age groups similar to ours (about 5 to 10 years) range between 0.73 and 0.88 (Krogsrud et al., 2016; Qiu et al., 2008; Rollins et al., 2010) and 0.54 and 0.74 (Colby et al., 2011; Krogsrud et al., 2016; Muftuler et al., 2012; Rollins et al., 2010; Tokariev et al., 2020), respectively. The corresponding values in ROI analysis studies range between 0.63 and 0.88 for CC (Genc et al., 2018; McGraw et al., 2002; Moon et al., 2011; Sadeghi et al., 2015; Schmithorst et al., 2008) and 0.49 and 0.72 for CST (Genc et al., 2018; Sadeghi et al., 2015). As discussed later, the

analysis method has a significant impact on the resultant values; for example, TBSS analysis focusses only on the core voxels of each tract and thus naturally provides higher FA values compared to analysis methods that also include the borderline voxels of the tract. This example highlights the difficulties in making between-study comparisons for diffusion scalar values. Our results indicate that the earlier research with less than 18 directions cannot be combined with future studies because of inconsistent biases and lack of precision in the numbers.

4.2 | Bias induced by reducing the number of diffusion gradient directions

In this study, decreasing the number of diffusion-encoding directions deteriorated both the accuracy and the precision of scalar values. The minimum number of directions was determined to be 18 with TBSS, and using more directions had no discernible advantage. Similar pattern was detected for scalar values in entire WM tract ROIs with non-skeletonised values. This is in line with prior investigations that have proposed that a minimum of 18 to 20 directions for FA values is required to yield reliable results (Jones, 2004; Ni et al., 2006; Papadakis et al., 2000).

We replicated the findings previously described in adult populations that using only six encoding diffusion directions result in overestimated FA values and at least 18 directions are required for repeatable results. Adult population-based reference values cannot be directly applied to paediatric DTI settings for several reasons. Firstly, there are structural and neurodevelopmental differences between children and adult brain, such as differences in the brain size and WM microstructure that are reflected generally as lower FA values in children. Secondly, problems with co-operation and subject motion during scanning are more frequent in paediatric MRI which may increase the requirement for data pre-processing and hence influence the results. Thirdly, as we discuss later on, methodological descriptions of paediatric studies often report removal of motion corrupted volumes, yet the final number of diffusion directions used in the analysis after pre-processing is frequently elusive. Thus, we believe it is essential to raise awareness of the importance of comprehensive reporting among researchers that work with paediatric DTI data.

Although using six diffusion-encoding directions overestimated the FA values, the result was not concordant when using 9 to 15 directions. Prior studies using real-life data have not provided estimations on scalar values with low number of directions spaced with narrow intervals. Systematic bias and increased variation induced

by lower number of directions can be partly explained by increased noise sensitivity. Lower SNR as a result of decreased number of diffusion directions has been shown to overestimate FA values (Barrio-Arranz et al., 2015; Chen et al., 2015; Heiervang et al., 2006; Papanikolaou et al., 2006). Additionally, inadequate inclusion of borderline voxels and problems with co-registration can also have significant influence on DTI results. Previous adult studies have reported the error being emphasised in areas with generally lower FA values (Chen et al., 2015; Sairanen et al., 2017). The fluctuation of values in our data was highlighted in tracts with low volumes and thus including fewer voxels, emphasising possible errors in the co-registration step or partial volume effects explaining part of the inaccuracy.

Diffusion parameters vary substantially along WM tracts (Johnson et al., 2014). As values are frequently reported as mean values across the entire tracts, fluctuations of scalar values inside a tract may be missed. One noteworthy region is the cingulum bundle with high number of crossing axons that cause voxel-wise variation between subjects, reflected as increased noise sensitivity (Sadeghi et al., 2015). Because cingulum also borders cerebrospinal fluid, minor misregistrations can also have substantial influence on scalar values (Sadeghi et al., 2015). Accordingly, accuracy of scalar estimates in the cingulum bundle with a low number of diffusion directions were inferior compared to other regions with similar sizes in our data. Similarly, CG was the only tract in which the FA values were detected to vary by decreasing the FA threshold from 0.20 to 0.15 or 0.10, yet the influence of the threshold and the number of directions on the resultant FA remained insignificant in formal statistical tests. As the TBSS skeleton with threshold of 0.15 extends outside WM tracts in multiple regions (supporting information 10), the use of threshold 0.20 is preferred (which is also the value used in the majority of the studies referred in the literature, Table 1).

TBSS is regarded as a standard approach for group comparisons of diffusion properties (Smith et al., 2006). Besides alleviating problems related to image misalignment and smoothing requirements, it has also been proposed to improve sensitivity and objectivity of results. However, interpretation of the results should be done with certain cautions, because TBSS also carries some limitations that should be carefully considered. As the method is automated, the output results after each step may not be checked and quality controlled. Additionally, TBSS alignment process has limited anatomical specificity and nearby tracts may be merged as skeletonisation process does not utilise directional information but FA maps instead, complicating the segregation of adjacent WM areas (Bach et al., 2014; Kindlmann et al., 2007).

Furthermore, the noise level and number of directions have been shown to influence the results of group comparisons with TBSS (Bach et al., 2014). A prior study has suggested the use of group-specific atlas as a target in the target registration step (Keihaninejad et al., 2012), which was also applied in our pipeline because of variation in brain sizes between children. The group-based template also alleviated the issues related to alignment to the atlas. We detected TBSS to reduce the variation of scalar values with low number of directions compared to ROI analysis of non-skeletonised values, which advocates the use of TBSS especially when only low number of diffusion directions is available. Addressing the details of optimising co-registration is beyond the scope of the current study. However, prior work on the topic might prove useful for such studies or optimising datasets with small amount of diffusion encoding data (de Groot et al., 2013; Zvitia et al., 2010).

We observed that the MD values were less dependent on the number of diffusion directions compared to FA. Previous studies comparing the reliability of FA and MD values have resulted in conflicting conclusions. Although proposing minimum of 20 directions for repeatable FA values, 30 directions were recommended for MD by Jones (2004). In the study by Bonekamp et al., ADC (apparent diffusion coefficient) was detected to be more reproducible when compared to FA when assessing intra- and inter-scanner repeatability (Bonekamp et al., 2007). In a multicentre DTI study, the overall concordance for FA was discovered to outweigh that of ADC values (0.96 vs 0.88) (Fox et al., 2012). MD values have more homogeneous distributions across the brain, compared to FA values. MD values have been previously reported to be insensitive to diffusion schemes and tensor orientations (Landman et al., 2007), whereas non-negligible dependence between MD and b values has been reported (Jones & Basser, 2004).

DTI data repeatability can be enhanced either by increasing the number of unique diffusion directions or by repetition and averaging. For example, in a simulation study (Jones, 2004), collection of maximum number of diffusion-encoding directions was recommended over repeated image acquisitions. Furthermore, increasing the number of directions showed most significant effect when SNR was low. Uniform sampling of diffusion directions was highlighted, as distortion of diffusion-encoding direction ratios may lead to overestimation of diffusion along a specific axis, producing bias in connectivity estimates (Jones, 2004). A comprehensive research concerning the effect of different diffusion tensor acquisition schemes with data collected with one adult participant and repeated imaging sessions was published previously (Landman et al., 2007). Orientation of diffusion tensor

was indicated to influence FA bias and precision, and this effect was mitigated by increased directional resolution (Landman et al., 2007). In our study, we collected the maximum number of unique directions (96) with no repetitions and maximised the angular resolution with even distribution of diffusion vectors on spherical surface by following uniformisation procedure described previously by Merisaari et al. (Merisaari et al., 2019). Additionally, the sampling of vectors in each of our subsets is unique among collected sequences. The subsets N6 to N60 were directly obtained from the N66 dataset prior to the application of motion correction steps. Hence, the evaluated N6 dataset has no strictly orthogonalised directions, as would be if the six orthogonal directions had been implemented without prior correction steps (without rotations because of, for example, motion correction). However, we believe that our results are applicable to such situations as well, noting that corresponding inaccuracies were detected with other low number of direction (N9 and N12).

The statistical significance of detected differences between separate direction sampling schemes is undeniable. In the current study, the absolute TBSS scalar values remained stable in major WM tracts with at least 12 directions (0.70 with 12 directions, 0.71 with 15 directions, 0.71 with 24 directions for GCC, and the corresponding values of 0.47, 0.45 and 0.47 for right CST) but more scattering appeared in tracts with lower FA values such as cingulate gyrus and uncinate fasciculus (corresponding values for right cingulate gyrus 0.31, 0.35 and 0.32 and for right uncinate fasciculus 0.47, 0.40 and 0.45). Thus, notable differences in absolute resultant scalar values are detected besides statistical differences emphasised in the peripheral areas with lower FA values.

Besides the diffusion direction sampling scheme, voxel size, resolution and SNR have also been found to influence the diffusion measures. Lower resolution resulted by increasing voxel size has been shown to underestimate FA values (Fujiwara et al., 2008; Papanikolaou et al., 2006). Brain volume at the age of 5 years has reached 90% of the adult brain volume (Lenroot & Giedd, 2006), as also demonstrated in our data by alignment of our study-specific template to adult FMRIB58_FA target, and therefore, the effects of relatively bigger voxel size are limited. However, a prior study has observed intracranial volume to influence FA and MD values in adult data even with the TBSS method (Takao et al., 2011). The variation was reasoned to derive partly from partial volume effects, which may also explain some of the variation in our data. Furthermore, decreased SNR has been shown to deteriorate the accuracy of FA values (Farrell et al., 2007). The results in our study were made after thorough pre-processing, which

we regard to resemble a situation where artefact-derived noise is limited to the minimum. Thus, the results are more distinct compared to situations where the effect of increasing the number of diffusion directions might be dampened by the low SNR.

4.3 | Within-scan head motion

We investigated the quantity and quality of the minor residual within-scan head motion after our extensive quality control protocol and exclusion of motion-corrupted diffusion gradients with both DTIprep and subsequent manual exclusion. The overall mean displacements between volumes remained low with values ranging below the size of voxels. The applied image analysis procedure in this study was regarded to be sufficient in removing the effects of motion on the DTI scalars.

With-scan motion has been indicated to distort diffusion imaging results with both underestimation and overestimation of FA values (Farrell et al., 2007; Jones & Basser, 2004; Landman et al., 2008; Tijssen et al., 2009). On the other hand, random removal of diffusion gradients has been shown to further decrease the precision and to introduce additional bias to DTI scalars. In a study by Ling et al., head motion was indicated to induce positive bias to FA and MD values in TBSS, voxel-wise and ROI analyses (Ling et al., 2012). Further, they demonstrated that random removal of corrupted diffusion gradients increased the bias on DTI scalars. Thus, elimination of diffusion gradients with gross movement artefacts requires caution, and both the sufficient number and uniform sampling of diffusion gradients after elimination must be ensured. We observed this by removing directions to reach subsets with N6 to N60 directions so that the angular resolution was maximised in each subset.

Only few paediatric DTI studies consider the impacts of the within-scan motion or removal of corrupted directions on the results, although within-scan motion is common in the paediatric imaging population. In studies included in our literature review, the routine eddy and motion corrections had been applied as a part of the image pre-processing in most of the reviewed studies, but quality control of diffusion volumes after pre-processing steps and removal of motion corrupted volumes was not consistently reported. Moreover, researchers do not often comment whether all diffusion gradients are accepted regardless of motion corruption or whether individual gradients are removed and still, if gradients are removed, whether the final amount of passed gradients is uniform between subjects. In our experience, automatic quality control procedure (DTIprep) was not alone accurate enough in removing all artefacts while keeping all

acceptable good directions with default settings, and thus the procedure was supplemented, and the results verified manually. It is possible to adjust the DTIprep settings to increase the sensitivity in detecting motion artefacts, but this was discovered to remove multiple volumes with no motion corruption. As we aimed to retain as many directions as possible, the combination of DTIprep and manual exclusion was found to result in the most efficient method. In a recent study, deep learning-based method was suggested as one solution in removing motion corruption from DTI data (Gong et al., 2021). As a promising method, it also requires a training diffusion weighted dataset with similar imaging parameters to study subjects, and thus needs to be considered during study design.

In our dataset, few children were able to lay still through the whole DTI scanning, partially explained by the long imaging time, which increases the possibility of within-scan movement. On average, 30% (95% CI 26–33%; range 0 to 64) of diffusion directions in our data ($n = 85$) were discarded during the motion and quality control steps when 96 directions were acquired. At least 50% of acquired directions were passed through our quality control protocol in 95% of the subjects in our study. Similar exclusion rates (13 to 29%) because of within-scan movement have been indicated in recent studies in this age group (Stephens et al., 2020; Theys et al., 2014). Modern imaging techniques and updated MRI hardware are also capable of mitigating motion artefacts by shortening image acquisition times, which alleviate problems with subject co-operation.

In summary, we recommend gathering twofold the number of required directions, that is 36 directions if aiming to 18, to include at least 95% of paediatric DTI participants. To increase between-study comparability, systematic reporting of exact DTI scalar values and the final number of diffusion-encoding gradients are recommended. As the last notion, the scope of the FinnBrain cohort study is to investigate the development of children and the participants also attended neuropsychological evaluation visits. Thus, we did not select our participants based on their abilities to lie still in the MR scanner but rather aimed to image all the children willing to attend the MRI substudy.

4.4 | Limitations

We investigated healthy, typically developing Finnish 5-year-olds and thus similar settings remain to be addressed in other age (especially younger children) and ethnic groups. We experimentally manipulated the number of diffusion-encoding directions across collected data without assessing the intra-scan and between-scan test-

retest reliability which are to be addressed in future studies.

The field map correction was not applied in our analysis pipeline. Generally, distortion correction is used to correct EPI distortion caused by magnetic field inhomogeneities. In our data, distortions were detected to be minor, and with the used methodology, we do not regard them to alter the results.

During our MRI protocol, T1 and T2 sequences were acquired prior to the DTI sequence, and were also repeated if necessary, which may have increased subject attrition. Thus, our study protocol was not totally optimised to achieve maximal subject inclusion rate for DTI sequences. Finally, our DTI sequences took 3×6 min, which is relatively long acquisition time as compared to many studies, because of more acquired diffusion-encoding directions. The length of the scan predisposes to within-scan motion.

5 | CONCLUSIONS

In the current study, we demonstrated that a low number of diffusion-encoding directions leads to decline in the accuracy and the precision of DTI scalar values and recommended that the minimum number of directions used should be 18 with TBSS analysis method. After excluding the motion corrupted directions both with automated and manual pre-processing, within-scan head motion was not detected to significantly affect the resultant scalar values. As head displacements are an unavoidable element in the brain imaging of awake paediatric participants, we suggest observing these aspects when designing the imaging protocols. Lastly, we encourage publishing of exact DTI scalar values in the field of paediatric brain imaging. In addition to contributing on formation of reference values that can possibly be applied to guide future clinical decision making, the reported scalar values could facilitate the comparison between separate studies.

ACKNOWLEDGEMENTS

The FinnBrain Birth Cohort Study (HK) was supported by the Jane and Aatos Erkko Foundation, the Academy of Finland and the Signe and Ane Gyllenberg Foundation. VK was supported by Cultural Foundation of Finland (#00190572) and the Finnish Medical Foundation. HM was supported by Cultural Foundation of Finland. ES was supported by Juho Vainio Foundation, Suomen aivosäätiö, Turunmaan Duodecim -seura.

CONFLICTS OF INTEREST

The authors declare that they have no competing interests.

ETHICS APPROVAL

The study was approved by the Ethics Committee of the Hospital District of Southwest Finland ([07.08.2018] §330, ETMK: 31/180/2011) and performed in accordance with the Declaration of Helsinki.

INFORMED CONSENT

Both parents of the participating child signed a written informed consent form.

AUTHOR CONTRIBUTION

VK participated in the recruitment, data collection, data pre-processing, analysis and manual quality control of the study subjects, statistical analysis and writing the manuscript. HM participated in designing and implementing data processing pipeline, statistical analyses and writing the manuscript. EPP, AC and ES participated in the recruitment and data collection and writing the manuscript. JDL and JS participated in designing the MR sequences and writing the manuscript. JJT and HK have designed the study and participated in writing the manuscript. HK and LK established the cohort and built infrastructure for carrying out the study. All authors have approved the final version of the manuscript.

PEER REVIEW

The peer review history for this article is available at <https://publons.com/publon/10.1111/ejn.15785>.

DATA AVAILABILITY STATEMENT

The Finnish law and ethical permissions do not allow sharing of the data used in this study.

ORCID

Venla Kumpulainen  <https://orcid.org/0000-0003-3375-5445>

Harri Merisaari  <https://orcid.org/0000-0002-8515-5399>

Elmo P. Pulli  <https://orcid.org/0000-0003-3871-8563>

REFERENCES

- Bach, M., Laun, F. B., Leemans, A., Tax, C. M. W., Biessels, G. J., Stieltjes, B., & Maier-Hein, K. H. (2014). Methodological considerations on tract-based spatial statistics (TBSS). *NeuroImage*, *100*, 358–369. <https://doi.org/10.1016/j.neuroimage.2014.06.021>
- Barrio-Arranz, G., De Luis-García, R., Tristán-Vega, A., Martín-Fernandez, M., & Aja-Fernandez, S. (2015). Impact of MR acquisition parameters on DTI scalar indexes: A tractography based approach. *PLoS ONE*, *10*(10), e0137905. <https://doi.org/10.1371/journal.pone.0137905>
- Basser, P. J., & Jones, D. K. (2002). Diffusion-tensor MRI: Theory, experimental design and data analysis - A technical review. *NMR in Biomedicine*, *15*(7–8), 456–467. <https://doi.org/10.1002/nbm.783>

- Basser, P. J., & Pierpaoli, C. (2011). Microstructural and physiological features of tissues elucidated by quantitative-diffusion-tensor MRI. *Journal of Magnetic Resonance*, 213(2), 560–570. <https://doi.org/10.1016/j.jmr.2011.09.022>
- Bonekamp, D., Nagae, L. M., Degaonkar, M., Matson, M., Abdalla, W. M. A., Barker, P. B., Mori, S., & Horská, A. (2007). Diffusion tensor imaging in children and adolescents: Reproducibility, hemispheric, and age-related differences. *NeuroImage*, 34(2), 733–742. <https://doi.org/10.1016/j.neuroimage.2006.09.020>
- Caroli, M., Pedro, M., de Castro, M., Lorient, S., Rouiller, O., Teillaud, M., & Wormser, C. (2010). *Robust and efficient Delaunay triangulations of points on or close to a sphere* (pp. 462–473). Springer Berlin Heidelberg, Berlin. https://doi.org/10.1007/978-3-642-13193-6_39
- Chen, Y., Tymofiyeva, O., Hess, C. P., & Xu, D. (2015). Effects of rejecting diffusion directions on tensor-derived parameters. *NeuroImage*, 109, 160–170. <https://doi.org/10.1016/j.neuroimage.2015.01.010>
- Chen, Z., Zhang, H., Yushkevich, P. A., Liu, M., & Beaulieu, C. (2016). Maturation along white matter tracts in human brain using a diffusion tensor surface model tract-specific analysis. *Frontiers in Neuroanatomy*, 10(9), 1–18. <https://doi.org/10.3389/fnana.2016.00009>
- Colby, J. B., Van Horn, J. D., & Sowell, E. R. (2011). Quantitative in vivo evidence for broad regional gradients in the timing of white matter maturation during adolescence. *NeuroImage*, 54(1), 25–31. <https://doi.org/10.1016/j.neuroimage.2010.08.014>
- de Groot, M., Vernooij, M. W., Klein, S., Ikram, M. A., Vos, F. M., Smith, S. M., Niessen, W. J., & Andersson, J. L. R. (2013). Improving alignment in tract-based spatial statistics: Evaluation and optimization of image registration. *NeuroImage*, 76, 400–411. <https://doi.org/10.1016/j.neuroimage.2013.03.015>
- Farah, R., Dudley, J., Hutton, J., & Horowitz-Kraus, T. (2020). Maternal Reading and fluency abilities are associated with diffusion properties of ventral and dorsal white matter tracts in their preschool-age children. *Brain and Cognition*, 140 (January), 105532. <https://doi.org/10.1016/j.bandc.2020.105532>
- Farrell, J. A. D., Landman, B. A., Jones, C. K., Smith, A., Prince, J. L., van Zijl, P. C., & Mori, S. (2007). Effects of SNR on the accuracy and reproducibility of DTI-derived fractional anisotropy, mean diffusivity, and principal eigenvector measurements at 1.5T. *Journal of Magnetic Resonance*, 26(3), 756–767. <https://doi.org/10.1002/jmri.21053>
- Fox, R. J., Sakaie, K., Lee, J. C., Debbins, J. P., Liu, Y., Arnold, D. L., Melhem, E. R., Smith, C. H., Philips, M. D., Lowe, M., & Fisher, E. (2012). A validation study of multicenter diffusion tensor imaging: Reliability of fractional anisotropy and diffusivity values. *AJNR. American Journal of Neuroradiology*, 33, 695–700. <https://doi.org/10.3174/ajnr.A2844>
- Fujiwara, S., Sasaki, M., Kanbara, Y., Inoue, T., Hirooka, R., & Ogawa, A. (2008). Feasibility of 1.6-mm isotropic voxel diffusion tensor tractography in depicting limbic fibers. *Neuroradiology*, 50(2), 131–136. <https://doi.org/10.1007/s00234-007-0317-y>
- Gao, W., Zhu, H., & Lin, W. (2009). A unified optimization approach for diffusion tensor imaging technique. *NeuroImage*, 44(3), 729–741. <https://doi.org/10.1016/j.neuroimage.2008.10.004>
- Genc, S., Malpas, C. B., Ball, G., Silk, T. J., & Seal, M. L. (2018). Age, sex, and puberty related development of the corpus callosum: A multi-technique diffusion MRI study. *Brain Structure and Function*, 223(6), 2753–2765. <https://doi.org/10.1007/s00429-018-1658-5>
- Genc, S., Malpas, C. B., Holland, S. K., Beare, R., & Silk, T. J. (2017). Neurite density index is sensitive to age related differences in the developing brain. *NeuroImage*, 148, 373–380. <https://doi.org/10.1016/j.neuroimage.2017.01.023>
- Giannelli, M., Cosottini, M., Michelassi, M. C., Lazzarotti, G., Belmonte, G., Bartolozzi, C., & Lazzari, M. (2010). Dependence of brain DTI maps of fractional anisotropy and mean diffusivity on the number of diffusion weighting directions. *Journal of Applied Clinical Medical Physics*, 11(1), 176–190. <https://doi.org/10.1120/jacmp.v11i1.2927>
- Gong, T., Tong, Q., Li, Z., He, H., Zhang, H., & Zhong, J. (2021). Deep learning-based method for reducing residual motion effects in diffusion parameter estimation. *Magnetic Resonance in Medicine*, 85(4), 2278–2293. <https://doi.org/10.1002/mrm.28544>
- Grohs, M. N., Reynolds, J. E., Dewey, D., & Lebel, C. (2018). Corpus callosum microstructure is associated with motor function in preschool children. *NeuroImage*, 183, 828–835. <https://doi.org/10.1016/j.neuroimage.2018.09.004>
- Heiervang, E., Behrens, T. E. J., Mackay, C. E., Robson, M. D., & Johansen-Berg, H. (2006). Between session reproducibility and between subject variability of diffusion MR and tractography measures. *NeuroImage*, 33, 867–877. <https://doi.org/10.1016/j.neuroimage.2006.07.037>
- Hermoye, L., Saint-Martin, C., Cosnard, G., Lee, S. K., Kim, J., Nassogne, M. C., Menten, R., Clapuyt, P., Donohue, P. K., Hua, K., Wakana, S., Jiang, H., Van Zijl, P. C. M., & Mori, S. (2006). Pediatric diffusion tensor imaging: Normal database and observation of the white matter maturation in early childhood. *NeuroImage*, 29(2), 493–504. <https://doi.org/10.1016/j.neuroimage.2005.08.017>
- Hutton, J. S., Dudley, J., Horowitz-Kraus, T., Dewitt, T., & Holland, S. K. (2020a). Associations between screen-based media use and brain white matter integrity in preschool-aged children. *JAMA Pediatrics*, 174(1), 1–10. <https://doi.org/10.1001/jamapediatrics.2019.3869>
- Hutton, J. S., Dudley, J., Horowitz-Kraus, T., DeWitt, T., & Holland, S. K. (2020b). Associations between home literacy environment, brain white matter integrity and cognitive abilities in preschool-age children. *Acta Paediatrica*, 109(7), 1376–1386. <https://doi.org/10.1111/apa.15124>
- Johnson, R. T., Yeatman, J. D., Wandell, B. A., Buonocore, M. H., Amaral, D. G., & Nordahl, C. W. (2014). Diffusion properties of major white matter tracts in young, typically developing children. *NeuroImage*, 88, 143–154. <https://doi.org/10.1016/j.neuroimage.2013.11.025>
- Jones, D. K. (2004). The effect of gradient sampling schemes on measures derived from diffusion tensor MRI: A Monte Carlo study. *Magnetic Resonance in Medicine*, 51, 807–815. <https://doi.org/10.1002/mrm.20033>
- Jones, D. K., & Basser, P. J. (2004). ‘Squashing peanuts and smashing pumpkins’: How noise distorts diffusion-weighted MR data. *Magnetic Resonance in Medicine*, 52(5), 979–993. <https://doi.org/10.1002/mrm.20283>

- Karlsson, L., Tolvanen, M., Scheinin, N. M., Uusitupa, H.-m., Korja, R., Ekholm, E., Tuulari, J. J., Pajulo, M., Huotilainen, M., Paunio, T., & Karlsson, H. (2017). Cohort profile: The FinnBrain birth cohort study (FinnBrain). *International Journal of Epidemiology*, *47*, 15–16j. <https://doi.org/10.1093/ije/dyx173>
- Keihaninejad, S., Ryan, N. S., Malone, I. B., Modat, M., Cash, D., Ridgway, G. R., Zhang, H., Fox, N. C., & Ourselin, S. (2012). The importance of group-wise registration in tract based spatial statistics study of neurodegeneration: A simulation study in Alzheimer's disease. *PLoS ONE*, *7*(11), 1–13. <https://doi.org/10.1371/journal.pone.0045996>
- Kindlmann, G., Tricoche, X., & Westin, C.-F. (2007). Delineating white matter structure in diffusion tensor MRI with anisotropy creases. *Medical Image Analysis*, *11*(5), 492–502. <https://doi.org/10.1016/j.media.2007.07.005>
- Krogsrud, S. K., Fjell, A. M., Tamnes, C. K., Grydeland, H., Mork, L., Due-tønnessen, P., Bjørnerud, A., Sampaio-baptista, C., Andersson, J., Johansen-berg, H., & Walhovd, K. B. (2016). Changes in white matter microstructure in the developing brain — A longitudinal diffusion tensor imaging study of children from 4 to 11 years of age. *NeuroImage*, *124*, 473–486. <https://doi.org/10.1016/j.neuroimage.2015.09.017>
- Kumpulainen, V., Lehtola, S. J., Tuulari, J. J., Silver, E., Copeland, A., Korja, R., Karlsson, H., Karlsson, L., Merisaari, H., Parkkola, R., Saunavaara, J., Lähdesmäki, T., & Scheinin, N. M. (2020). Prevalence and risk factors of incidental findings in brain MRIs of healthy neonates—The FinnBrain birth cohort study. *Frontiers in Neurology*, *10*(8), 1347. <https://doi.org/10.3389/fneur.2019.01347>
- Landman, B. A., Farrell, J. A., Huang, H., Prince, J. L., & Mori, S. (2008). Diffusion tensor imaging at low SNR: Non-monotonic behaviors of tensor contrasts. *Magnetic Resonance Imaging*, *26*(6), 790–800. <https://doi.org/10.1016/j.mri.2008.01.034>
- Landman, B. A., Farrell, J. A. D., Jones, C. K., Smith, S. A., Prince, J. L., & Mori, S. (2007). Effects of diffusion weighting schemes on the reproducibility of DTI-derived fractional anisotropy, mean diffusivity, and principal eigenvector measurements at 1.5T. *NeuroImage*, *36*, 1123–1138. <https://doi.org/10.1016/j.neuroimage.2007.02.056>
- Le Bihan, D., Poupon, C., Amadon, A., & Lethimonnier, F. (2006). Artifacts and pitfalls in diffusion MRI. *Journal of Magnetic Resonance Imaging*, *24*(3), 478–488. <https://doi.org/10.1002/jmri.20683>
- Lebel, C., Gee, M., Camicioli, R., Wieler, M., Martin, W., & Beaulieu, C. (2012). Diffusion tensor imaging of white matter tract evolution over the lifespan. *NeuroImage*, *60*(1), 340–352. <https://doi.org/10.1016/j.neuroimage.2011.11.094>
- Lebel, C., & Deoni, S. (2018). The development of brain white matter microstructure. *NeuroImage*, *182*, 207–218. <https://doi.org/10.1016/j.neuroimage.2017.12.097>
- Lebel, C., Treit, S., & Beaulieu, C. (2017). A Review of Diffusion MRI of Typical White Matter Development from Early Childhood to Young Adulthood. *NMR in Biomedicine*, *32*, 1–23. <https://doi.org/10.1002/nbm.3778>
- Lebel, C., Walton, M., Letourneau, N., Giesbrecht, G. F., Kaplan, B. J., & Dewey, D. (2016). Prepartum and postpartum maternal depressive symptoms are related to Children's brain structure in preschool. *Biological Psychiatry*, *80*(11), 859–868. <https://doi.org/10.1016/j.biopsych.2015.12.004>
- Lee, S. J., Zhang, J., Neale, M. C., Styner, M., Zhu, H., & Gilmore, J. H. (2019). Quantitative tract-based white matter heritability in 1- and 2-year-old twins. *Human Brain Mapping*, *40*(4), 1164–1173. <https://doi.org/10.1002/hbm.24436>
- Lenroot, R. K., & Giedd, J. N. (2006). Brain development in children and adolescents: Insights from anatomical magnetic resonance imaging. *Neuroscience and Biobehavioral Reviews*, *30*(6), 718–729. <https://doi.org/10.1016/j.neubiorev.2006.06.001>
- Ling, J., Merideth, F., Caprihan, A., Pena, A., Teshiba, T., & Mayer, A. R. (2012). Head injury or head motion? Assessment and quantification of motion artifacts in diffusion tensor imaging studies. *Human Brain Mapping*, *33*(1), 50–62. <https://doi.org/10.1002/hbm.21192>
- Loenneker, T., Klaver, P., Bucher, K., Lichtensteiger, J., Imfeld, A., & Martin, E. (2011). Microstructural development: Organizational differences of the fiber architecture between children and adults in dorsal and ventral visual streams. *Human Brain Mapping*, *32*, 935–946. <https://doi.org/10.1002/hbm.21080>
- McGraw, P., Liang, L., & Provenzale, J. M. (2002). Evaluation of Normal age-related changes in anisotropy during infancy and childhood as shown by diffusion tensor imaging. *American Journal of Roentgenology*, *179*(6), 1515–1522. <https://doi.org/10.2214/ajr.179.6.1791515>
- Merisaari, H., Tuulari, J. J., Karlsson, L., Scheinin, N. M., Parkkola, R., Saunavaara, J., Lähdesmäki, T., Lehtola, S. J., Keskinen, M., Lewis, A. C., Evans, A. C., & Karlsson, H. (2019). Test-retest reliability of diffusion tensor imaging metrics in neonates. *NeuroImage*, *197*, 598–607. <https://doi.org/10.1016/j.neuroimage.2019.04.067>
- Millman, K. J., & Aivazis, M. (2011). Python for scientists and engineers. *Computing in Science & Engineering*, *13*, 9–12. <https://doi.org/10.1109/MCSE.2011.36>
- Moon, W.-j., Provenzale, J., Sarikaya, B., Ihn, Y. K., Morlese, J., Chen, S., & DeBellis, M. D. (2011). Diffusion tensor imaging assessment of white matter maturation in childhood and adolescence. *AJR. American Journal of Roentgenology*, *197*(3), 704–712. <https://doi.org/10.2214/AJR.10.6382>
- Mori, S., Oishi, K., Jiang, H., Jiang, L., Li, X., Akhter, K., Hua, K., Faria, A. V., Mahmood, A., Woods, R., Toga, A. W., Pike, G. B., Neto, P. R., Evans, A., Zhang, J., Huang, H., Miller, M. I., van Zijl, P., & Mazziotta, J. (2008). Stereotaxic white matter atlas based on diffusion tensor imaging in an ICBM template. *NeuroImage*, *40*(2), 570–582. <https://doi.org/10.1016/j.neuroimage.2007.12.035>
- Moura, L., Kempton, M., Barker, G., Salum, G., Gadelha, A., Pan, P. M., Hoexter, M., del Aquilla, M. A. G., Picon, F. A., Anés, M., Otaduy, M. C. G., Amaro, E., Rohde, L. A., McGuire, P., Bressan, R. A., Sato, R. J., & Jackowski, A. P. (2016). Age-effects in white matter using associated diffusion tensor imaging and magnetization transfer ratio during late childhood and early adolescence. *Magnetic Resonance Imaging*, *34*(4), 529–534. <https://doi.org/10.1016/j.mri.2015.12.021>
- Muftuler, L. T., Davis, E. P., Buss, C., Solodkin, A., Su, M. Y., Head, K. M., Hasso, A. N., & Sandman, C. A. (2012). Development of white matter pathways in typically developing

- preadolescent children. *Brain Research*, 1466, 33–43. <https://doi.org/10.1016/j.brainres.2012.05.035>
- Ni, H., Kavcic, V., Zhu, T., Ekholm, S., & Zhong, J. (2006). Effects of number of diffusion gradient directions derived diffusion tensor imaging indices in Human brain. *AJNR. American Journal of Neuroradiology*, 27, 1776–1781.
- Oguz, I., Farzinfar, M., Matsui, J., Budin, F., Liu, Z., Gerig, G., Johnson, H. J., & Styner, M. (2014). DTIPrep: Quality control of diffusion-weighted images. *Frontiers in Neuroinformatics*, 8, 1–11. <https://doi.org/10.3389/fninf.2014.00004>
- Oishi, K., Zilles, K., Amunts, K., Faria, A., Jiang, H., Li, X., Akhter, K., Hua, K., Woods, R., Toga, A. W., Pike, G. B., Rosa-Neto, P., Evans, A., Zhang, J., Huang, H., Miller, M. I., van Zijl, P. C. M., Mazziotta, J., & Mori, S. (2008). Human brain white matter atlas: Identification and assignment of common anatomical structures in superficial white matter. *NeuroImage*, 43(3), 447–457. <https://doi.org/10.1016/j.neuroimage.2008.07.009>
- Papadakis, N. G., Murrills, C. D., Hall, L. D., Huang, C. L. H., & Adrian Carpenter, T. (2000). Minimal gradient encoding for robust estimation of diffusion anisotropy. *Magnetic Resonance Imaging*, 18(6), 671–679. [https://doi.org/10.1016/S0730-725X\(00\)00151-X](https://doi.org/10.1016/S0730-725X(00)00151-X)
- Papanikolaou, N., Karampekios, S., Papadaki, E., Malamas, M., Maris, T., & Gourtsoyiannis, N. (2006). Fractional anisotropy and mean diffusivity measurements on Normal human brain: Comparison between low- and high-resolution diffusion tensor imaging sequences. *European Radiology*, 16, 187–192. <https://doi.org/10.1007/s00330-005-2833-7>
- Pierpaoli, C., Jezzard, P., Basser, P. J., Barnett, A., & Di Chiro, G. (1996). Diffusion tensor MR imaging of the human brain. *Radiology*, 201(3), 637–648. <https://doi.org/10.1148/radiology.201.3.8939209>
- Qiu, D., Tan, L. H., Zhou, K., & Khong, P. L. (2008). Diffusion tensor imaging of normal white matter maturation from late childhood to Young adulthood: Voxel-wise evaluation of mean diffusivity, fractional anisotropy, radial and axial diffusivities, and correlation with reading development. *NeuroImage*, 41(2), 223–232. <https://doi.org/10.1016/j.neuroimage.2008.02.023>
- Reynolds, J. E., Grohs, M. N., Dewey, D., & Lebel, C. (2019). Global and regional white matter development in early childhood. *NeuroImage*, 196, 49–58. <https://doi.org/10.1016/j.neuroimage.2019.04.004>
- Rollins, N. K., Glasier, P., Seo, Y., Morriss, M. C., Chia, J., & Wang, Z. (2010). Age-related variations in white matter anisotropy in school-age children. *Pediatric Radiology*, 40, 1918–1930. <https://doi.org/10.1007/s00247-010-1744-1>
- Sadeghi, N., Nayak, A., Walker, L., Okan Irfanoglu, M., Albert, P. S., Pierpaoli, C., & Brain Development Cooperative Group. (2015). Analysis of the contribution of experimental bias, experimental noise, and inter-subject biological variability on the assessment of developmental trajectories in diffusion MRI studies of the brain. *NeuroImage*, 109, 480–492. <https://doi.org/10.1016/j.neuroimage.2014.12.084>
- Sairanen, V., Kuusela, L., Sipilä, O., Savolainen, S., & Vanhatalo, S. (2017). A novel measure of reliability in diffusion tensor imaging after data rejections Due to subject motion. *NeuroImage*, 147(February 2016), 57–65. <https://doi.org/10.1016/j.neuroimage.2016.11.061>
- Sarkar, S., Craig, M. C., Dell'Acqua, F., O'Connor, T. G., Catani, M., Deeley, Q., Glover, V., & Murphy, D. G. M. (2014). Prenatal stress and limbic-prefrontal white matter microstructure in children aged 6–9 years: A preliminary diffusion tensor imaging study. *The World Journal of Biological Psychiatry*, 15, 346–352. <https://doi.org/10.3109/15622975.2014.903336>
- Scherf, K. S., Thomas, C., Doyle, J., & Behrmann, M. (2014). Emerging structure – Function relations in the developing face processing system. *Cerebral Cortex*, 24, 2964–2980. <https://doi.org/10.1093/cercor/bht152>
- Schmithorst, V. J., Holland, S. K., & Dardzinski, B. J. (2008). Developmental differences in white matter architecture between boys and girls. *Human Brain Mapping*, 29, 696–710. <https://doi.org/10.1002/hbm.20431>
- Seunarine, K. K., Clayden, J. D., Jentschke, S., Muñoz, M., Cooper, J. M., Chadwick, M. J., Banks, T., Vargha-Khadem, F., & Clark, C. A. (2016). Sexual dimorphism in white matter developmental trajectories using tract-based spatial statistics. *Brain Connectivity*, 6(1), 37–47. <https://doi.org/10.1089/brain.2015.0340>
- Shrout, P. E., & Fleiss, J. L. (1979). Intraclass correlations: uses in assessing rater reliability. *Psychological Bulletin*, 86(2), 420–428. <https://doi.org/10.1037/0033-2909.86.2.420>
- Smith, S. M. (2002). Fast robust automated brain extraction. *Human Brain Mapping*, 17(3), 143–155. <https://doi.org/10.1002/hbm.10062>
- Smith, S. M., Jenkinson, M., Johansen-Berg, H., Rueckert, D., Nichols, T. E., Mackay, C. E., Watkins, K. E., Ciccarelli, O., Cader, Z., Matthews, P. M., & Behrens, T. E. J. (2006). Tract-based spatial statistics: Voxelwise analysis of multi-subject diffusion data. *NeuroImage*, 31(4), 1487–1505. <https://doi.org/10.1016/j.neuroimage.2006.02.024>
- Stephens, R. L., Langworthy, B. W., Short, S. J., Girault, J. B., Styner, M. A., & Gilmore, J. H. (2020). White matter development from birth to 6 years of age: A longitudinal study. *Cerebral Cortex*, 30(12), 6152–6168. <https://doi.org/10.1093/cercor/bhaa170>
- Swartz, J., Carrasco, M., Wiggins, J. L., Thomason, M. E., & Monk, C. S. (2015). Age-related changes in the structure and function of prefrontal cortex-amygdala circuitry in children and adolescents: A multi-modal imaging approach. *NeuroImage*, 86, 212–220. <https://doi.org/10.1016/j.neuroimage.2013.08.018.Age-related>
- Takao, H., Hayashi, N., Inano, S., & Ohtomo, K. (2011). Effect of Head size on diffusion tensor imaging. *NeuroImage*, 57(3), 958–967. <https://doi.org/10.1016/j.neuroimage.2011.05.019>
- Taki, Y., Thyreau, B., Hashizume, H., Sassa, Y., Takeuchi, H., Wu, K., Kotozaki, Y., Nouchi, R., Asano, M., Asano, K., Fukuda, H., & Kawashima, R. (2013). Linear and curvilinear correlations of brain white matter volume, fractional anisotropy, and mean diffusivity with age using voxel-based and region-of-interest analyses in 246 healthy children. *Human Brain Mapping*, 34(8), 1842–1856. <https://doi.org/10.1002/hbm.22027>
- Tamnes, C. K., Østby, Y., Fjell, A. M., Westlye, L. T., Due-Tønnessen, P., & Walhovd, K. B. (2010). Brain maturation in adolescence and Young adulthood: Regional age-related changes in cortical thickness and white matter volume and

- microstructure. *Cerebral Cortex*, 20(3), 534–548. <https://doi.org/10.1093/cercor/bhp118>
- Theys, C., Wouters, J., & Ghesquière, P. (2014). Diffusion tensor imaging and resting-state functional MRI-scanning in 5- and 6-year-old children: Training protocol and motion assessment. *PLoS ONE*, 9(4), 1–7. <https://doi.org/10.1371/journal.pone.0094019>
- Tijssen, R. H. N., Jansen, J. F. A., & Backes, W. H. (2009). Assessing and minimizing the effects of noise and motion in clinical DTI at 3 T. *Human Brain Mapping*, 30(8), 2641–2655. <https://doi.org/10.1002/hbm.20695>
- Tokariev, M., Vuontela, V., Perkola, J., Lönnberg, P., Lano, A., Andersson, S., Metsäranta, M., & Carlson, S. (2020). A protocol for the analysis of DTI data collected from Young children. *MethodsX*, 7, 100878. <https://doi.org/10.1016/j.mex.2020.100878>
- Wier, R., Aleksonis, H. A., Pearson, M. M., Cannistraci, C. J., Anderson, A. W., Kuttesch, J. F., Compas, B. E., & Hoskinson, K. R. (2019). Fronto-limbic white matter microstructure, behavior, and emotion regulation in survivors of pediatric brain tumor. *Journal of Neuro-Oncology*, 143(3), 483–493. <https://doi.org/10.1007/s11060-019-03180-5>
- Young, J. M., Vandewouw, M. M., Mossad, S. I., Morgan, B. R., Lee, W., Smith, M. L., Sled, J. G., & Taylor, M. J. (2019). White matter microstructural differences identified using multi-shell diffusion imaging in six-year-old children born very preterm. *NeuroImage: Clinical*, 23, 101855. <https://doi.org/10.1016/j.nicl.2019.101855>
- Yu, Q., Peng, Y., Kang, H., Peng, Q., Ouyang, M., Slinger, M., Hu, D., Shou, H., Fang, F., & Huang, H. (2020). Differential white matter maturation from birth to 8 years of age. *Cerebral Cortex*, 30(4), 2673–2689. <https://doi.org/10.1093/cercor/bhz268>
- Zvitia, O., Mayer, A., Shadmi, R., Miron, S., & Greenspan, H. K. (2010). Co-registration of white matter tractographies by adaptive-mean-shift and Gaussian mixture modeling. *IEEE Transactions on Medical Imaging*, 29(1), 132–145. <https://doi.org/10.1109/TMI.2009.2029097>

SUPPORTING INFORMATION

Additional supporting information can be found online in the Supporting Information section at the end of this article.

How to cite this article: Kumpulainen, V., Merisaari, H., Copeland, A., Silver, E., Pulli, E. P., Lewis, J. D., Saukko, E., Saunavaara, J., Karlsson, L., Karlsson, H., & Tuulari, J. J. (2022). Effect of number of diffusion-encoding directions in diffusion metrics of 5-year-olds using tract-based spatial statistical analysis. *European Journal of Neuroscience*, 1–26. <https://doi.org/10.1111/ejn.15785>